AD-A120 867 RESEARCH OF MICROSTRUCTURALLY DEVELOPED TOUGHENING MECHANISMS IN CERAMICS..(U) ROCKWELL INTERNATIONAL THOUSAND OAKS CA SCIENCE CENTER F F LANGE ET AL. 1/1

UNCLASSIFIED OCT 82 SC5117.13TR N00014-77-C-0441 F/G 11/2 NL

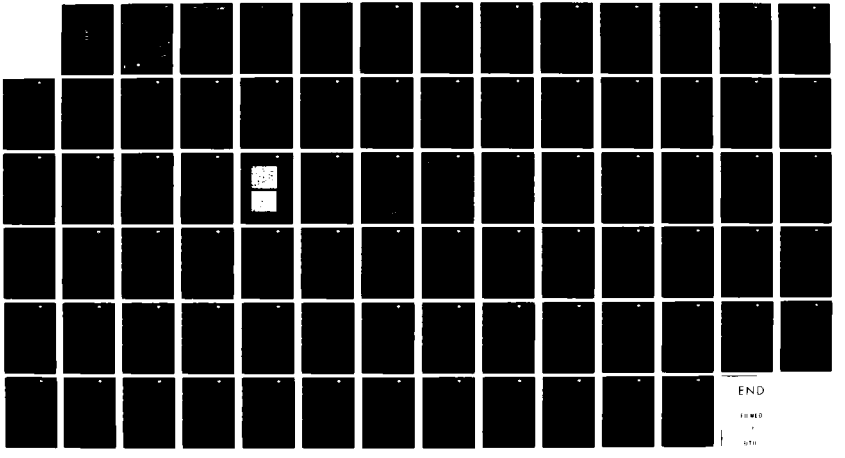

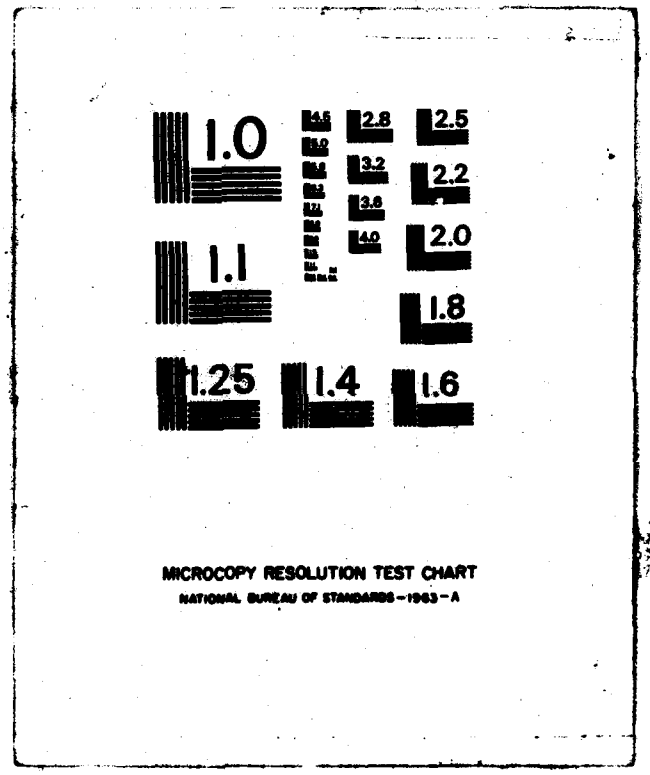
1.0
1.1
1.25
1.4
1.6
2.8
3.2
3.6
4.0
2.5
2.2
2.0
1.8
MICROCOPY RESOLUTION TEST CHART
NATIONAL BUREAU OF STANDARDS-1963-A

(12)

Copy No. 133

# RESEARCH OF MICROSTRUCTURALLY DEVELOPED TOUGHENING MECHANISMS IN CERAMICS

TECHNICAL REPORTS NO. 13, 14, 15, 16
FOR PERIOD JUNE 1, 1982 THROUGH MAY 31, 1982

CONTRACT NO. N00014-77-C-0441
PROJECT NO. 032-574(471)

PART 1: DETERMINATION OF RESIDUAL SURFACE STRESSES DUE TO GRINDING IN POLYCRYSTALLINE $Al_2O_3$ (SC5117.13TR)

PART 2: FACTORS INFLUENCING THE RESIDUAL SURFACE STRESSES DUE TO A STRESS-INDUCED PHASE TRANSFORMATION (SC5117.14TR)

PART 3: COMPRESSIVE SURFACE STRENGTHENING OF BRITTLE MATERIALS (SC5117.15TR)

PART 4: TRANSFORMATION TOUGHENING: THERMODYNAMIC APPROACH TO PHASE RETENTION AND TOUGHENING (SC5117.16TR)



Prepared for:
Office of Naval Research
Arlington, VA 22217

F. F. Lange





Rockwell International
Science Center

UNCLASSIFIED

SECURITY CLASSIFICATION OF THIS PAGE (When Data Entered)

| REPORT DOCUMENTATION PAGE | | READ INSTRUCTIONS BEFORE COMPLETING FORM |
|---|---|---|
| 1. REPORT NUMBER | 2. GOVT ACCESSION NO. AD-A120867 | 3. RECIPIENT'S CATALOG NUMBER |
| 4. TITLE (and Subtitle) RESEARCH OF MICROSTRUCTURALLY DEVELOPED TOUGHENING MECHANISMS IN CERAMICS | | 5. TYPE OF REPORT & PERIOD COVERED Technical Report #13 for the period 6/1/81 thru 5/31/82 |
| | | 6. PERFORMING ORG. REPORT NUMBER SC5117.13TR |
| 7. AUTHOR(s) F.F. Lange | | 8. CONTRACT OR GRANT NUMBER(s) N00014-77-C-0441 |
| 9. PERFORMING ORGANIZATION NAME AND ADDRESS Rockwell International Science Center 1049 Camino Dos Rios Thousand Oaks, CA 91360 | | 10. PROGRAM ELEMENT, PROJECT, TASK AREA & WORK UNIT NUMBERS 032-574-(471) |
| 11. CONTROLLING OFFICE NAME AND ADDRESS Office of Naval Research Department of the Navy Arlington, VA 22217 | | 12. REPORT DATE October, 1982 |
| | | 13. NUMBER OF PAGES 73 |
| 14. MONITORING AGENCY NAME & ADDRESS(if different from Controlling Office) | | 15. SECURITY CLASS. (of this report) Unclassified |
| | | 15a. DECLASSIFICATION/DOWNGRADING SCHEDULE |

16. DISTRIBUTION STATEMENT (of this Report)

Approved for public release; distribution unlimited.

17. DISTRIBUTION STATEMENT (of the abstract entered in Block 20, if different from Report)

18. SUPPLEMENTARY NOTES

19. KEY WORDS (Continue on reverse side if necessary and identify by block number)

Residual surface stress, x-ray diffraction, surface grinding, ceramics, stress-induced phase transformation, $Al_2O_3/ZrO_2$ composites, strengthening, transformation toughening, fracture mechanics, crack closure.

20. ABSTRACT (Continue on reverse side if necessary and identify by block number)

An x-ray diffraction technique has been used to measure the residual surface stresses induced by surface grinding in $Al_2O_3$ and in transformation-toughened $Al_2O_3/ZrO_2$ composites. For the $Al_2O_3$, compressive stresses in the range 135 to 170 MPa were measured and were found to extend to a depth $\leq$ 15 μm. It is believed that the compressive layer is produced by the elastic/plastic interaction of the abrasive grains with the ceramics. In the $Al_2O_3/ZrO_2$ composites, compressive surface stresses are a result of

DD FORM 1 JAN 73 1473 EDITION OF 1 NOV 65 IS OBSOLETE

UNCLASSIFIED

SECURITY CLASSIFICATION OF THIS PAGE (When Data Entered)

micron

the $ZrO_2^n$ phase transformation, which is induced by the stresses during grinding. Residual compressive surfaces stresses up to ≈ 1 GPa were measured. The role of the volume fraction of $ZrO_2^n$, grain size and stabilizer oxide content in controlling the phase transformation are discussed, and their influence on the residual surface stress were measured. It was found that the volume fraction of $ZrO_2^n$ primarily controlled the magnitude of the compressive surface stress, but that other factors such as grain size influenced the depth of the compressive zone.

Finally, a fracture mechanics model is presented that allows the strengthening due to these residual stresses to be predicted. The model, which allows for crack closure effects, showed that the strengthening depends on the ratio of the compressive zone depth to surface crack length, and on the strength of the material in the absence of residual stresses.

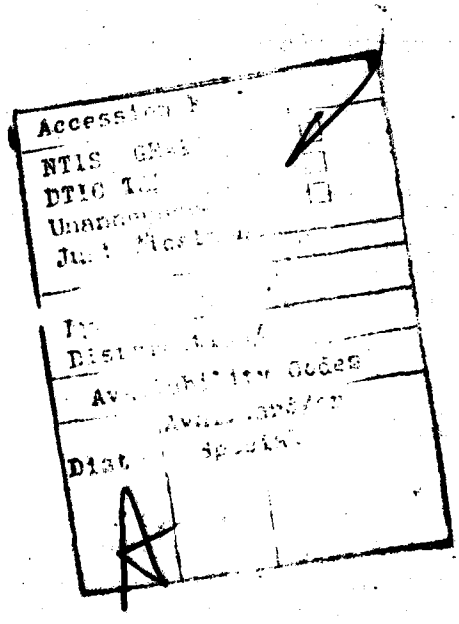

TECHNICAL REPORT NO. 13

# DETERMINATION OF RESIDUAL SURFACE STRESSES DUE TO GRINDING IN POLYCRYSTALLINE $Al_2O_3$

F.F. Lange, M.R. James and D.J. Green

Rockwell International
Science Center

SC5117.13TR

# DETERMINATION OF RESIDUAL SURFACE STRESSES DUE TO GRINDING IN POLYCRYSTALLINE $Al_2O_3$

F.F. Lange, M.R. James and D.J. Green

Rockwell International Science Center
1049 Camino Dos Rios
Thousand Oaks, CA 91360

## ABSTRACT

Residual surface stresses introduced into polycrystalline $Al_2O_3$ during diamond grinding (320 grit) were examined with an x-ray diffraction technique commonly used for metals. Compressive stresses, estimated to be in the range of 135 MPa to 170 MPa and to extend < 15 μm in depth, were observed at the surface. It is believed that the compressive surface layer coincides with the plastic layer produced by the elastic/plastic interaction of the abrasive grains with the ceramic. The results are discussed with regard to the effect of the compressive layer on the extension of surface cracks.

## 1. Introduction

Grinding, a common processing step for ceramics, introduces both plastic deformation and cracks into the material adjacent to the surface. The elastic/plastic interaction of abrasive grains with the ceramic surface has been considered analogous to a series of closely-spaced sliding, single-point indenters. As reviewed by Lawn and co-workers,[1,2] a sharp indenter plastically deforms a small volume of material, which is proportional in size to the indenter impression. When the applied load is greater than a critical value, the sharp indenter also produces lateral (approximately parallel to the surface) and radial (normal to the surface) cracks. Intersecting lateral cracks are believed responsible for material removal during grinding; whereas the radial

cracks will lead to strength degradation. Rice et al.[3] have shown that two types of radial cracks exist within the groove produced by the plowing abrasive grains: 1) closely spaced cracks that traverse the groove produced by slip-stick and 2) longitudinal cracks which overlap one another along the length of the groove. The overlapping, longitudinal radial cracks produce the greatest strength degradation, resulting in a strength anisotropy when tensile strength is measured parallel and perpendicular to the grinding direction.

The residual surface stresses produced by the overlapping plastically-deformed volume elements associated with each grinding groove are of greatest concern in the present investigation. For the indentation produced by an isolated, sharp indenter, the material within the plastically deformed volume is in a state of compression and exerts tensile stresses on the radial crack fronts both at the surface and in the interior. These residual tensile stresses aid in crack extension when an external tensile load is applied to induce failure.[4] However, when the plastically-deformed volume elements overlap one another, i.e., the suspected case for grinding, one would suspect that the complete surface would be plastically deformed and in a state of compression. If this were the case, the portions of the cracks within the compressive layer would be closed. These partially compressed cracks would be less effective in degrading strength than currently suspected from results of single-point indentation studies.[4]

The objective of this work was to determine if surface stresses are produced by surface grinding, and to estimate their magnitude and depth.

## 2. Approach

Surface residual stress measurements were made using an x-ray diffraction technique that is ideally suited for very shallow (~ few μm) depths and commercially employed by the metals industry. Authoratative reviews exist on this technique,[5,6] which requires a polycrystalline sample so that a given set of (hkl) diffracting planes can be examined as a function of their angular rotation with respect to the specimen's surface. This is accomplished by

tilting the specimen and determining the Bragg angle for the chosen (hkl) planes as a function of the tilt angle. A change in the Bragg angle infers a surface strain. Conversion of the measured strain into surface stress is most easily accomplished by assuming isotropic elasticity. To partially compensate for anisotropic behavior along the particular (hkl) planes, the elastic constants specific to that plane are used rather than bulk values of the aggregate. Denoting these "x-ray elastic constants" as $S_2$, isotropic elasticity theory yields $S_2 = (1 + \nu)/E$, where $\nu$ and E are Poisson's ratio and Young's modulus, respectively. The conversion also assumes that the surface is in a state of biaxial stress to the depth penetrated by the x-rays and that the principle strain axes are coplanar with the surface.

The x-ray elastic constants for the <hkl> direction can either be calculated with knowledge of the single crystal elastic compliance constants (see Nye[7] or Dolle[8]) or determined by direct measurement. The experimental determination used here involved strain gauging a bar specimen (approximately 0.3 × 0.6 × 3 cm) that had been annealed to help ensure minimal surface stresses. Surface strain determined with the strain gauge was first correlated to an applied surface stress by loading the bar specimen in 4-pt bending with an Instron Testing machine. The strain-gauged specimen was then placed in another 4-pt flexural loading jig mounted on the x-ray diffractometer to obtain correlation between the applied surface stress (as determined from the calibrated strain gauge) and the surface strain, as determined by the change in 2θ for the chosen (hkl), to obtain the elastic constants for the chosen <hkl> direction.

The particular computer-automated instrumentation and technique used here to determine surface stresses is similar to that described previously.[9] Each measurement was carried out using eight tilt angles (0° to 45°). The peak of the diffraction profile at each tilt angle was determined by the apex of a least-squares parabola fit to the top portion of the profile. The profiles were very broad (> 3° 2θ full width, half maximum) and symmetric about the apex. To ensure that grinding did not introduce errors due to the principle strain components being inclined to the surface,[8] some mesurements were carried out

at both positive and negative tilt angles and gave identical results. Typically, a single measurement of residual stress took three hours.

Hot-pressed $Al_2O_3$ (1500°C/2 hr), with an average grain size of 2 μm was chosen for the surface stress determinations.[10] Initially, both Cu-radiation ($\lambda$ = 1.542Å) and Cr-radiation ($\lambda$ = 2.291Å) were used for the study, but preliminary work quickly showed the need for the shallower penetrating Cr-radiation.* The (602) diffraction peak was chosen for the Cu-radiation ($2\theta \approx 142°$) and the (119) peak for the Cr-radiation ($2\theta \approx 135°$). The x-ray elastic constants was determined for the respective <hkl> directions as described above. It was also calculated for the <119> direction using the $Al_2O_3$ single crystal compliance constants.[11] Based on the counting statistical accuracy[9] of the (119) peak, the precision of the $2\theta$ determination was calculated to be ± 0.030°. This corresponds to a statistical precision of ± 45 MPa when the (119) diffraction peak was used for surface stress determinations.

Three different bar specimens (approximately 0.3 × 0.6 × 1.0 cm) were ground on four sides with a 320 grit diamond wheel removing ~ 25 μm of material with each pass.† Surface stresses in the direction of grinding were determined on one ground specimen with both Cu and Cr radiation. The second ground specimen was only examined with Cr radiation; subsequent determinations were made after 5 μm and then 10 μm of surface material was removed by polishing with 3 μm diamond paste. The third specimen was annealed at 1500°C/1 hr prior to surface stress examination. Surface stress determinations were repeated 2 or 3 times at different positions on the bar for each condition examined and the results averaged.

---

*Using the mass absorption coefficient for $Al_2O_3$ for either Cr or Cu radiation, and the possible path length for the given $2\theta$, 50% of the radiation is diffracted from an $Al_2O_3$ surface layer of 8 μm for Cr-radiation and 26 μm for Cu-radiation.

†Elgin, Inc., CD320R100BF-1/8-C4

## 3. Results

Table I lists the experimentally determined and calculated value of $E/(1 + \nu)$. The experimental value for the <119> direction was ~ 25% lower than the value calculated from the single crystal compliance constants.

Table II summarizes the surface stress results calculated with the experimentally determined value of $E/(1 + \nu)$. Values would be ~ 25% greater if single crystal results for $E/(1 + \nu)$ were used instead. Note that all surface stresses are compressive. Compressive stresses on the ground surface are substantial, viz ~ 135 MPa (to 170 MPa if single crystal results for $E/(1 + \nu)$ are used), whereas the 1 hr anneal reduced the stresses to within the limits

Table I

Values of $E/(1 + \nu)$

| Radiation | Crystal Direction | $E/(1 + \nu)$ (GPa) Experimental | Calculated |
|---|---|---|---|
| Cu | <602> | 212 | -- |
| Cr | <119> | 246 | 313 |

Table II

Surface Stress Determinations

| Specimen | Radiation | Surface Treatment | Average Compressive Surface Stress* (MPa) |
|---|---|---|---|
| 1 | Cu | Ground | 35 ± 16 (3)** |
| 1 | Cr | Ground | 125 ± 7 (2) |
| 2 | Cr | Ground | 145 ± 21 (2) |
| 2 | Cr | 5 μm Removed | 70 ± 28 (2) |
| 2 | Cr | 10 μm Removed | 83 ± 56 (2) |
| 3 | Cr | Annealed | 29 ± 49 (3) |

* Calculated using experimental value of $E/(1 + \nu)$.
** ( ) Number of determinations.

of experimental error. Results of the deeper penetrating Cu-radiation (50% diffracted within a depth of 25 μm from surface) and Cr-radiation (50% from a 8 μm depth) and those obtained by polishing the surface to remove up to 10 μm of material suggest that a majority of the compressive stresses are within a surface layer ≤ 10 μm deep. Also note that most of the deviations are within that indicated from statistical counting errors (± 45 MPa) indicating that the stress state is uniform over the surface. The results of polishing suggest that even this procedure introduces a small amount of compressive residual stress.

## 4. Discussion

It has been shown that surface grinding with a commonly used diamond finishing wheel (320 grit) can produce substantial (135 to 170 MPa) compressive surface stresses that extend to a significant depth (≤ 10 μm). It is reasonable to suspect that the compressive surface stresses arise due to the formation of a plasticity-deformed surface layer produced by the elastic/plastic interaction of closely spaced [illegible] as discussed in the introduction. That is, [illegible] layer is in a state of compression.

It is suspected that the surface compressive stresses will influence the catastrophic behavior of brittle ceramics. The surface compressive stress will reduce the stress intensity factor of a surface crack subjected to an applied tensile stress. Fracture mechanics have shown that the magnitude of this effect depends on the ratio of the crack length (c) to surface compressive layer depth (t):

Using the results for single point indentation studies, one can estimate c/t. Recent results of Anstis et al.[13] for the elastic/plastic interaction of the Vickers indenter, suggest the following relation:

$$c/t = \alpha(a/d) = 0.09\alpha \left(H^{1/4}E^{1/2}K_c^{-1}P^{1/4}\right)^{2/3} \qquad (1)$$

where d = indentation half-diagonal (radius of the grinding groove), H = material hardness, E = Young's Modulus, P = indenter load (grinding wheel's

vertical load), $K_c$ = critical stress intensity factor. For $Al_2O_3$,[10] H = 18 GPa, E = 400 GPa, $K_c$ = 4.9 MPa $m^{1/2}$,

$$a/t \simeq 2\ \alpha[P]^{1/6} \quad , \tag{2}$$

where P is the vertical load of the diamond wheel in kilograms. Under normal grinding conditions P < 1 Kgm, thus $a/t \sim 2\alpha$. Examining the extreme cases when $t = d$ ($\alpha = 1$) and $t > a$ ($\alpha < 1/2$), i.e., the case where the crack is completely imbedded within the compressive layer, Green and Lange's[12] analysis indicates that the strength increase due to the compressive layer for the cases where $\alpha = 1$ and $\alpha < 1/2$ are 30% and 100% of the compressive stress, respectively. For the $Al_2O_3$ used in the present work, the average flexural strength of ground specimens is 610 MPa.[10] Data reported in Table II indicates a compressive stress of 135 to 170 MPa. Thus, if surface cracks were strength controlling and if the compressive stress could be removed (e.g., by annealing) without healing the surface cracks, one would expect that the average strength to decrease by a stress in the range of ~ 45 MPa ($\alpha = 1$, 30% of 135 MPa) to 170 MPa ($\alpha < 1/2$, 100% of 170 MPa).

The above discussion assumed that the closely spaced grinding grooves are uniform in depth and thus produced a plastic layer of uniform thickness. Surface topography measurements suggest that this is not the case for present day grinding wheels, viz, one or more grooves are much deeper than others. That is, the larger cracks associated with the deeper grooves will dominate strength determinations and the compressive surface layer may have less effect then indicated above.

In conclusion, it has been shown that significant surface compressive stresses result from surface grinding, i.e., the plastic interaction of the grinding wheel ameliorates the detrimental elastic interaction (surface cracks).

## ACKNOWLEDGEMENT

This work was supported by the Office of Naval Research, Contract No. N00014-77-C-0441.

## REFERENCES

1. B.R. Lawn and T.R. Wilshaw, "Indentation Fracture: Principles and Applications," J. Mat. Sci. 10[6] 1049-81 (1975).

2. B.R. Lawn and D.B. Marshall, "Indentation Fracture and Strength Degradatin in Ceramics," pp. 205-29, in Fracture Mechanics of Ceramics Vol. 3. Ed. by R.C. Bradt, D.P.H. Hasselman and F.F. Lange, Plenum Press (1978).

3. R.W. Rice, J.J. Mecholsky, Jr., and P.F. Becher, "The Effect of Grinding Correction on Flaw Character and Strength of Single Crystal and Polycrystalline Ceramics," J. Mat. Sci. 16[4] 853-62 (1981).

4. D.B. Marshall, B.R. Lawn and P. Chantikul, "Residual Stress Effects in Sharp Contrast Cracking," Part 2 Strength Degradation," J. Mat. Sci. 14[9], 2225-35 (1979).

5. M.E. Hilley, J.A. Larson, C.F. Jatczak and R.E. Ricklefs (eds.), Residual Stress Measurements by X-ray Diffrction, SAE Information Report J784a, SAE, Warrendale, Pennsylvania.

6. M.R. James and J.B. Cohen, "The Measurement of Residual Stresses by X-Ray Diffraction Techniques," pp. 1-62 in Treatise on Materials Science and Technology, 19A, ed. H. Hermon, Academic Press, NY, (1980).

7. J.F. Nye, Physical Properties of Crystals, pp. 143-5, Oxford at the Clarendon Press, London, 1957.

8. H. Dolle, "The Influence of Multiaxial Stress States, Stress Gradients and Elastic Anisotropy on the Evaluation of Residual Stresses by X-Rays," J. Apply. Cryst., 12, 489-501 (1979).

9. M.R. James and J.B. Cohen, "Study of the Precision of X-ray Stress Analysis," Denver Conference on Advances in X-ray Analysis, 20 (ed. H.F. McMurdie), Kendal/Hunt Publishing Co., Dubuque, Iowa, 291-307 (1977).

10. F.F. Lange, "Transformation Toughening: Part 4, Fabrication, Fracture Toughness and Strength of $Al_2O_3$-$ZrO_2$ Composites," J. Mat. Sci. 17[1], 247-54 (1982).

11. G. Simmons and H. Wang, Single Crystal Elastic Constants and Calculated Aggregate Properties: A Handbook, p. 146, MIT Press, Cambridge, Mass (1971).

12. D.J. Green and F.F. Lange, "Influence of Residual Surface Stresses on the Strength of $ZrO_2$ Ceramics," Paper 28-BN-79F, Fall Meeting of Basic Science and Nuclear Divisions of the American Ceramic Society, New Orleans, 1979.

13. G.R. Anstis, P. Chantikul, B.R. Lawn, and D.B. Marshall, "A Critical Evaluation of Indentation Techniques for Measuring Fracture Toughness: I, Direct Crack Measurements," J. Am. Ceram. Soc. 64[9] 533-38 (1981).

TECHNICAL REPORT NO. 14

# FACTORS INFLUENCING THE RESIDUAL SURFACE STRESSES DUE TO A STRESS-INDUCED PHASE TRANSFORMATION

D.J. Green, F.F. Lange and M.R. James

# FACTORS INFLUENCING THE RESIDUAL SURFACE STRESSES DUE TO A STRESS-INDUCED PHASE TRANSFORMATION

D.J. Green, F.F. Lange and M.R. James

Rockwell International Science Center
1049 Camino Dos Rios
Thousand Oaks, CA 91360

## 1. Introduction

Residual surface compressive stresses are known to increase the strength of glasses and ceramics. Commercial glasses are strengthened by either tempering or ion-exchange methods. Kirchner et al.[1-3] have shown that the surfaces of different single phase ceramics can be placed in compression by a) diffusing ions which decrease the thermal expansion of the surface layer, b) glazing, and c) thermal quenching. Lange[4] demonstrated that the surface of a two-phase (or multiphase) ceramic can be placed in compression when the minor phase increases its molar volume by a reaction which proceeds from the surface (e.g., oxidation, etc.). Molar volume changes can also be produced by structural transformations. Garvie et al.[5,6] were the first to demonstrate that a compressive stress arises on the ground surfaces of polycrystalline cubic $ZrO_2$ materials containing precipitates of tetragonal $ZrO_2$. The $ZrO_2(t) \rightarrow ZrO_2(m)$ transformation, which involves a volume increase of ~3 to 5%, was induced by the grinding stresses. As demonstrated by Garvie and others, ceramics containing $ZrO_2(t)$ can be made stronger by surface grinding.*[5-11]

The strengthening due to compressive surface stresses is a result of the residual stresses opposing the applied stresses. Green[12] has shown that

*The $ZrO_2(t) \rightarrow ZrO_2(m)$ also increases fracture toughness, which also strengthens materials containing $ZrO_2(t)$.

the stress intensity factor of a surface crack subjected to both a residual compressive surface stress and an applied tensile stress depends on three factors: 1) the magnitude of the residual compressive stress, 2) the residual stress profile with respect to distance from the surface, and 3) the crack length (c) to compressive layer thickness (t) ratio (c/t). For a given residual stress, the stress intensity factor is minimized (and strength maximized) when the crack is fully embedded within a uniform compressive layer ($c/t < 1$).[12] Thus, if one could engineer the magnitude, profile and depth of the compressive surface stress, one could minimize the effect of surface cracks on strength.

The goal of this investigation was to determine those factors that effect the magnitude, profile and depth of the compressive layer introduced by a structural phase transformation. As it will be described, the experimental portion of this work utilizes an x-ray diffraction technique to directly determine the state of residual stress.

## 2. Stress-Induced Structural Phase Transformations

If the surface of a large body undergoes a molar volume increase to a depth t, the biaxial compressive stress within this layer can be approximated by[13]

$$\sigma_c \simeq \frac{1}{3} \left( \frac{\Delta V}{V} \right) \frac{E V_i}{(1-\nu)} \quad , \tag{1}$$

where $\Delta V/V$ is the molar volume increase, $V_i$ is the volume fraction of material with an increased molar volume, E is the elastic modulus, and $\nu$, Poisson's ratio. When the compressive layer is small compared to the size of the body, tensile stresses, much smaller in magnitude relative to $\sigma_c$ exist at depths greater than t.

The molar volume change of interest here is associated with a structural transformation induced by external stresses applied to the surface as, e.g., through the action of impinging, high velocity particles, or that of an abrasive grinding wheel. The depth to which material transforms will depend on both the magnitude of the applied stress as a function of the distance from the

surface, and the critical applied stress required to induce the transformation. This critical applied stress can be related to the thermodynamic parameters associated with the constrained transformation and the material's microstructure with the following analysis.

Let us assume that the volume element undergoing the stress-induced transformation is an individual grain or inclusion that is surrounded by a continuous matrix, which can be other grains of the same phase or another phase. The high temperature phase, constrained by the elastic matrix to low temperatures, will be labeled t, and its transformed structure will labeled m, in reference to the $ZrO_2$ (tetragonal) → $ZrO_2$ (monoclinic) transformation discussed in the experimental portion. Because the strain energy associated with the constrained transformation can be larger than the free energy gained by the structural transformation, the high temperature structure can be retained to much lower temperature than can be achieved in the unconstrained state. The retention of the high temperature phase also depends on size of the volume element undergoing the transformation. The size effect is due to the energetics of surface phenomena that accompany the transformation (viz. twinning and microcracking), and the fact that the free energy and strain energy terms scale differently with respect to the surface terms. The energetics of this transformation can be summarized with[14]

$$\Delta G_{t\rightarrow m} = -|\Delta G_c| + \Delta U_{se} f + \frac{6\Sigma\gamma g}{D} \quad , \tag{2}$$

where $\Delta G_{t\rightarrow m}$ is the total change in free energy, $|\Delta G_c|$ is the magnitude of the free energy change associated with the unconstrained transformation (the negative size preceding this term denotes that the transformation would be spontaneous in the unconstrained case), $\Delta U_{se}$ is the strain energy change, and (1-f) is the reduction of strain energy due to accompanying surface phenomena that relieve either shear strains (twinning) or dilatational strains (microcracking). The term $6\Sigma\gamma g/D$, is a summation of all the surface phenomena that accompany the transformation, viz., the interfacial energy change $(\gamma_m - \gamma_t g_s)A_m$, the energy of twin boundaries, $\gamma_T g_T A_m$, and the energy of microcracks, $\gamma_c g_c A_m$. In these terms, $\gamma$ denotes energy per unit areas associated with the particular surface, and g

denotes the area of the particular surface normalized by the interfacial area of the transformed inclusion, $A_m$ (e.g., $g_s = A_t/A_m$, where $A_t$ is the interfacial area of the high temperature phase). Since the units of Eq. (2) are energy/volume, the surface terms must be divided by the transformed volume ($\pi D^3/6$), hence the size of the transformed inclusion is present in the denominator of the surface term in Eq. (2). The surface term(s) dictate a size effect, i.e., a critical size exists below which the transformation is not spontaneous ($\Delta G_{t \to m} > 0$):

$$D_C = (|\Delta G_c| - \Delta U_{se} f)/(6 \Sigma \gamma g) \quad . \tag{3}$$

Let us now examine the case where a stress field must be applied to cause the transformation to be spontaneous. The types of stresses required are those that help reduce the constraint imposed by the elastic matrix. For example, if the transformation increases the volume of the inclusions hydrostatic tensile stresses would help relieve the matrix constraint. When the transformation occurs under an applied stress, the external loading system does work:[15]

$$W = \sigma^a_{ij} \, \varepsilon^t_{ij} \quad , \tag{4}$$

where $\sigma^a_{ij}$ are the components of the applied stress tensor, and $\varepsilon^t_{ij}$ are the components of the transformational strain tensor. Since this work aids the transformation, it is a negative term as shown by

$$\Delta G_{t \to m} = -|\Delta G_c| + \Delta U_{se} f + \frac{6 \Sigma \gamma g}{D} - W \quad . \tag{5}$$

The minimum amount of work required to induce the transformation is obtained from $\Delta G_{t \to m} = 0$, or

$$W = -|\Delta G_c| + \Delta U_{se} f + \frac{6 \Sigma \gamma g}{D} \quad . \tag{6}$$

To reduce the complexity of Eq. (6) (for the general case, W contains 6 terms), let us assume that the transformation can be defined by one strain

component, e.g., a simple isotropic volume increase where $\varepsilon_{ij} = \varepsilon_t = \Delta V/(3V)$, when i = nd $\varepsilon_{ij} = 0$ for $i \neq j$. For this case, the smallest applied hydrostatic tensile stress required to induce the transformation is given by

$$\sigma_a^c = (-|\Delta G_c| + \Delta U_{se} f + \frac{6\Sigma\gamma g}{D})/\varepsilon_t \quad , \tag{7}$$

i.e., $\sigma_a^c$ is the critical applied stress required to induce the transformation. Equation (7) shows that the conditions to cause the transformation to become spontaneous without an applied stress occurs when the summation in the numerator $\to 0$. Let us now examine the effects of each term in Eq. (7) holding all others constant. First, Eq. (7) shows that as $|\Delta G_c| \to 0$ (the case where the two unconstrained phases are in equilibrium), $\sigma_a^c$ increases to approach $(U_{se} f + \frac{6\Sigma\gamma g}{D})/\varepsilon_t$. Second, for the transformation involving a simple volume change, $\Delta U_{se} = k\varepsilon_t^2/6$, (16) where k is the effective elastic modulus of the two phases given by

$$k = \frac{2E_m E_i}{(1+\nu_m)E_i + 2(1-2\nu_i)E_m} \quad . \tag{8}$$

This relation shows that as the elastic modulus of the matrix (m) is increased, $\sigma_a^c$ is increased. The third effect is concerned with the inclusion size (D). Its effect can better be illustrated by combining Eqs. (3) and (7) to obtain

$$\sigma_a^c = \frac{(-|\Delta G_c| + \Delta U_{se} f)(1 - \frac{D_c}{D})}{\varepsilon_t} \quad . \tag{9}$$

Equation (9) shows that as $D \to 0$, $\sigma_a^c \to \infty$, and as $D \to D_c$, $\sigma_a^c \to 0$.

We are now able to examine the effect of $|\Delta G_c|$, $\Delta U_{se}$ and D on the transformation depth, (t), for a given type of surface stressing condition. Since the stress applied to the surface decreases with increasing depth, the stress at some depth >t will be insufficient to satisfy the stress required to induce the transformation. The above arguments show that this depth can be maximized when the high temperature phase is just on the verge of transforma-

tion, i.e., where just a little stress is required to induce the transformation. This condition exists when $|\Delta G_c|$ is large, viz. $|\Delta G_c| \rightarrow \Delta U_{se} + 6\Sigma\gamma g/D$, $\Delta U_{se}$ is small, viz. when the elastic modulus of the constraining matrix is low, and when $D \rightarrow D_c$. Conversely, the above arguments show that the depth of the transformed surface layer is minimized when $|\Delta G_c| \rightarrow 0$, $\Delta U_{se}$ is large (viz. large matrix modulus) and $D \rightarrow 0$.

## 3. Experimental

Surface surface stress measurements were carried out with a variety of two phase, $Al_2O_3/ZrO_2$ materials in which the $ZrO_2$ was retained in its tetragonal structure during cooling from the fabrication temperature. Surface stresses were introduced by surface grinding with a 320 grit diamond wheel to induce the $ZrO_2(t) \rightarrow ZrO_2(m)$ transformation. The effect of changing the volume fraction of the $ZrO_2(t)$ ($V_1$), the chemical-free energy change ($|\Delta G_c|$) of the unconstrained $ZrO_2(t) \rightarrow ZrO_2(m)$ transformation and the grain size of the $ZrO_2(t)$ (D) on the residual compressive stress were systematically investigated.

### 3.1 Surface Stress Determination

Surface residual stress measurements were made using an x-ray diffraction technique ideally suited for very shallow (microns) depths and commercially employed by the metals industry. Authoratative reviews exist on this technique.[17,18] The technique requires a polycrystalline sample so that a given set of (hkl) diffracting planes can be examined as a function of their angular rotation with respect to the specimen's surface. This is accomplished by tilting the specimen and determining the Bragg angle for the chosen (hkl) planes as a function of the tilt angle. A change in the Bragg angle infers a surface strain. Conversion of the measured strain into surface stress is most easily accomplished by assuming isotropic elasticity. To partially compensate for anistotropic behavior along the particular (hkl) planes, the elastic constants specific to that plane are used rather than bulk values of the aggregate. Denoting these "x-ray elastic constants" as $S_2$, isotropic elasticity

theory yields $S_2 = (1 + \nu)/E$, where $\nu$ and E are Poission's ratio and Young's modulus, respectively. The conversion also assumes that the surface is in a state of constant biaxial stress to the depth penetrated by the x-rays, and that the principle strain axes are coplanar with the surface.

The x-ray elastic constants for the (hkl) direction can either be calculated with knowledge of the single crystal elastic compliance constants (see Nye[19] or Dolle[20]) or determined by direct measurement. The experimental determination used here involved strain-gauging a bar specimen (approximately 0.3 x 0.6 x 3 cm) that had been annealed to help ensure minimal surface stresses. Surface strain determined with the strain gauge was first correlated to an applied surface stress by loading the bar specimen in 4-pt bending with an Instron testing machine. The strain-gauged specimen was then placed in another 4-pt flexural loading jig mounted on the x-ray diffractometer to obtain correlation between the applied surface stress (as determined from the calibrated strain gauge), and the surface strain as determined by the change in 2θ for the chosen (hkl) to obtain the elastic constants for the chosen (hkl) direction.

The particular computer-automated instrumentation and technique used here to determine surface stresses is similar to that described previously.[21] Each measurement was carried out using eight tilt angles (0° to 45°). The peak of the diffraction profile at each tilt angle was determined by the apex of a least-squares parabola fit to the top portion of the profile. The profiles were very broad (>3° 2θ full width half maximum) and symmetric about the apex. To ensure that grinding did not introduce errors due to the principle strain components being inclined to the surface,[20] some measurements were carried out at both positive and negative tilt angles and gave identical results. Typically, a single measurement of residual stress took three hours.

For the present work, both CuKα ($\lambda$ = 1.542Å) and CrKα ($\lambda$ = 2.291Å), radiations were used in this study. The $Al_2O_3$ (602) diffraction peak was chosen for the Cu radiation (2θ ≈ 142°), and the (119) peak chosen for the Cr radiation (2θ = 135°). Table 1 lists the penetration depths (normal to surface) for both CuKα and CrKα at 2θ = 142° and 135°, respectively, calculated for the mass absorption coefficients and densities of the $Al_2O_3/ZrO_2$ composites for the

Table 1

Depth ( m) of Diffracted X-rays vs $ZrO_2$

| Radiation | Volume % $ZrO_2$* | | | | | | | % Diffracted |
|---|---|---|---|---|---|---|---|---|
| | 7.5 | 15 | 20 | 30 | 40 | 52 | 60 | |
| CuKα | | | | 12.8 | | | | 50 |
| (2θ ≈ 142°) | | | | 114.0 | | | | 95 |
| CrKα | 6.5 | 5.5 | 4.9 | 4.1 | 3.5 | 3.0 | 2.6 | 50 |
| (2θ ≈ 135°) | 28.1 | 23.6 | 21.2 | 17.6 | 15 | 12.9 | 11.3 | 95 |

*Alloy additions to $ZrO_2$ (viz $Y_2O_3$ or $CeO_2$) not taken into account in calculations.

different composites investigated with each radiation. This table illustrates that CuKα is much more penetrating than CrKα, and the penetration depth decreases with increasing vol % $ZrO_2$.

It should be noted that the surface stress determination is a mean value of stresses integrated over the depth penetrated by the radiation used (weighed by an exponential function due to absorption). If the residual surface stress is not constant with increasing depth and/or its depth is less than the depth penetrated by diffraction x-rays, one would expect different mean values for different characteristic x-rays.

Table 2 lists the values of $E/(1 + \nu)$ for the two sets of planes obtained by the experimental method described above, and through calculations using single crystal compliance constants.[22] Note that the calculated value of $E/(1+\nu)$ is ~ 25 % greater.

Table 2

Values of $E/(1 + \nu)$

| Radiation | Crystal Direction | $E/(1 + \nu)$ (GPa) Experimental | Calculated |
|---|---|---|---|
| Cu | <602> | 212 | -- |
| Cr | <119> | 246 | 313 |

## 3.2 Materials

One series of $Al_2O_3/ZrO_2$ composites containing 30 volume percent (v/o) $ZrO_2$ were investigated in which the $ZrO_2$ contained between 9 and 22 mole percent (m/o) $CeO_2$. The unconstrained t → m transformation temperature decreases with increasing m/o $CeO_2$.[23] Thus, increasing $CeO_2$ additions decreases the room temperature value of $|\Delta G_c|$. The fabrication and sintering (1600°C/2 hr) of these materials are reported elsewhere.[23]

A second $Al_2O_3/ZrO_2$ series was fabricated to contain different v/o $ZrO_2$. For this series, $Y_2O_3$ was used as the alloy addition, which was incorporated by the manufacturer.* The $Y_2O_3$ content was increased with increasing v/o $ZrO_2$ in the composite, viz. 1.37 m/o $Y_2O_3$ for composites containing 7.5 and 15 v/o $ZrO_2$, 2.50 m/o $Y_2O_3$ for the 30, 40 and 50 v/o $ZrO_2$ composites, and 3.65 m/o $Y_2O_3$ for the 60 v/o $ZrO_2$ composite.§ Since the elastic modulus of the composites decreases with increasing $ZrO_2$ v/o, the m/o $Y_2O_3$ must be increased to retain the tetragonal structure, as discussed elsewhere.[14] A colloidal/filtration route was used to consolidate milled composite powders in this series similar to that described elsewhere.[24] Sintering was carried out at 1600°C/2 hr.

Three other $Al_2O_3/ZrO_2$ composites containing 7.5 v/o $ZrO_2$ (no $Y_2O_3$), 6.6 v/o $ZrO_2$ (2.0 m/o $Y_2O_3$), and 30 v/o $ZrO_2$ (2.0 m/o $Y_2O_3$) were also investigated. These materials were hot-pressed (1500°C/ 2 hr) as described elsewhere.[25]

## 3.3 Experiments

All surface grinding was carried out with a 320 grit diamond wheel† using a Dual Surface grinding machine. Approximately 10 μm of material was removed during each pass. Bar specimens (approximately 0.3 x 0.6 x 1.0 cm) were

*Zircar Products Inc., Florida, N.Y.
§$Y_2O_3$ content determined by Spectrochemical Laboratories Inc., Pittsburgh, PA.
†Elgin, Inc., CD320-R100-BF-1/8-C4

used. The crystal structure of the $ZrO_2$ adjacent to the surface was determined by x-ray diffraction analysis. The approximate monoclinic/tetragonal ratio was determined with the($1\bar{1}1$) monoclinic/(111) tetragonal peak height ratio.

The first experiments, carried out with the hot-pressed materials, did not involve surface stress measurements. These experiments simply involved careful polishing (3 μm diamond paste) of the ground surface, and determining the monoclinic/tetragonal ratio as a function in the depth of material removed. CuKα radiation was used for these measurements.

Surface stress measurements were carried out on the $Al_2O_3/ZrO_2$ (30 v/o) composite series containing the different $CeO_2$ alloy additions. All specimens were ground during the same period. Both CuKα and CrKα radiation was used for surface stress determinations. Surface stress determinations were redetermined for several specimens with CrKα radiation after annealing at 1650°C/2 hr.

To determine the effect of grain size on surface stresses, the sintered $Al_2O_3$/30 v/o $ZrO_2$ (2.50 m/o $Y_2O_3$) material was cut into a number of bar specimens, each of which were heat treated for 2, 8, 16 and 24 hrs at 1650°C to increase the as-fabricated $ZrO_2$ grain size. Grain size distributions were determined on SEM micrographs using a Quantimet Image Analyzer. Approximately 600 grains were examined for each heat treatment. All but one of these specimens were then ground during the same period for surface stress determinations. Two specimens (annealed 0 hr and 24 hr, then ground) were carefully polished to remove, in subsequent steps, between 2 to 4 μm of surface material. Surface stresses were redetermined after each polishing step in an attempt to determine the depth of the surface stress layer and the stress profile.

Surface stress determinations were carried out for the series surface-ground, sintered composites containing increasing v/o of $ZrO_2$.

## 4. Results

### 4.1 Surface Phase Analysis

Table 3 lists the monoclinic/tetragonal phase ratio for as-sintered (or as-annealed) and as-ground surfaces. For the series containing the $CeO_2$ alloying addition to $ZrO_2$ (Table 3a), note that the $ZrO_2$ in the sintered materials alloyed with both 9 and 10 m/o $CeO_2$ was not fully tetragonal. Also for the same series, the monoclinic content of ground surfaces with either CuKα or CrKα decreased with increasing m/o $CeO_2$.

Table 3a

Monoclinic/Tetragonal Phase Ratio for $Al_2O_3$/30 v/o $ZrO_2$ Series Alloyed with $CeO_2$

| $CeO_2$ Content | Ratio of Peak Intensities (111)m/(111)t | | |
|---|---|---|---|
| | Sintered Surface | Ground Surface | |
| | CuKα* | CuKα* | CrKα |
| 9 | 0.33 | 0.97 | 1.07 |
| 10 | 0.29 | 0.60 | 0.82 |
| 13 | <0.02 | 0.17 | 0.15 |
| 14 | <0.02 | 0.085 | 0.11 |
| 15 | <0.02 | 0.064 | 0.070 |
| 17 | <0.02 | 0.035 | 0.045 |
| 18 | <0.02 | 0.027 | <0.02 |
| 20 | <0.02 | <0.02 | <0.02 |
| 22 | <0.02 | <0.02 | <0.02 |

* ± 0.02.

For the second series listed in Table 3b, the materials most sensitive to transformation, both during fabrication and subsequent surface grinding, were those in which the $ZrO_2$ was alloyed with only 1.37 m/o $Y_2O_3$. A 20 v/o $ZrO_2$ composite was also fabricated with the same $ZrO_2$ (+1.37 m/o $Y_2O_3$) powder, but it

contained approximately equal proportions of monoclinic and tetragonal $ZrO_2$ and was deemed unsuitable for consistant experimentation. Note that surface grinding generally increased the monoclinic content of the surface.

Figure 1 illustrates the m/t intensity ratio for the three hot-pressed materials which were sequentially polished to remove surface material and re-examined for phase content. Note the difference in the monoclinic depth for the 7.5 v/o $ZrO_2$ (0 m/o $Y_2O_3$) and 6.6 v/o $ZrO_2$ (+2 m/o $Y_2O_3$). The depth of the transformed layer for the material alloyed with $Y_2O_3$ is much shallower relative to that containing no $Y_2O_3$. Also note that the 30 v/o $ZrO_2$ composite had a transformed layer intermediate in depth to the other two.

Table 3b

Monoclinic/Tetragonal Phase Ratio

| v/o $ZrO_2$ | m/o $Y_2O_3$ | Sinter (Anneal) Condition | Ratio of Peak Intensity (111)m/(111)t | | |
|---|---|---|---|---|---|
| | | | Sintered Surface | Ground Surface | |
| | | | CuKα* | CuKα* | CrKα |
| 7.5 | 1.37 | 1600°C/2 hr | 0.02 | 0.22 | 0.14 |
| 15 | 1.37 | 1600°C/2 hr | 0.09 | 0.38 | 1.01 |
| 30 | 2.5 | 1600°C/2 hr | <0.02 | 0.06 | 0.21 |
| 30 | 2.5 | (1650°C/2 hr) | <0.02 | 0.09 | ** |
| 30 | 2.5 | (1650°C/8 hr) | <0.02 | 0.09 | ** |
| 30 | 2.5 | (1650°C/16 hr) | 0.03 | 0.08 | ** |
| 30 | 2.5 | (1650°C/24 hr) | <0.02 | 0.10 | ** |
| 40 | 2.5 | 1600°C/2 hr | <0.02 | <0.02 | <0.02 |
| 50 | 2.5 | 1600°C/2 hr | <0.02 | 0.07 | ** |
| 60 | 3.65 | 1600°C/2 hr | <0.02 | 0.05 | 0.12 |

* ± 0.02.
** - data not recorded.

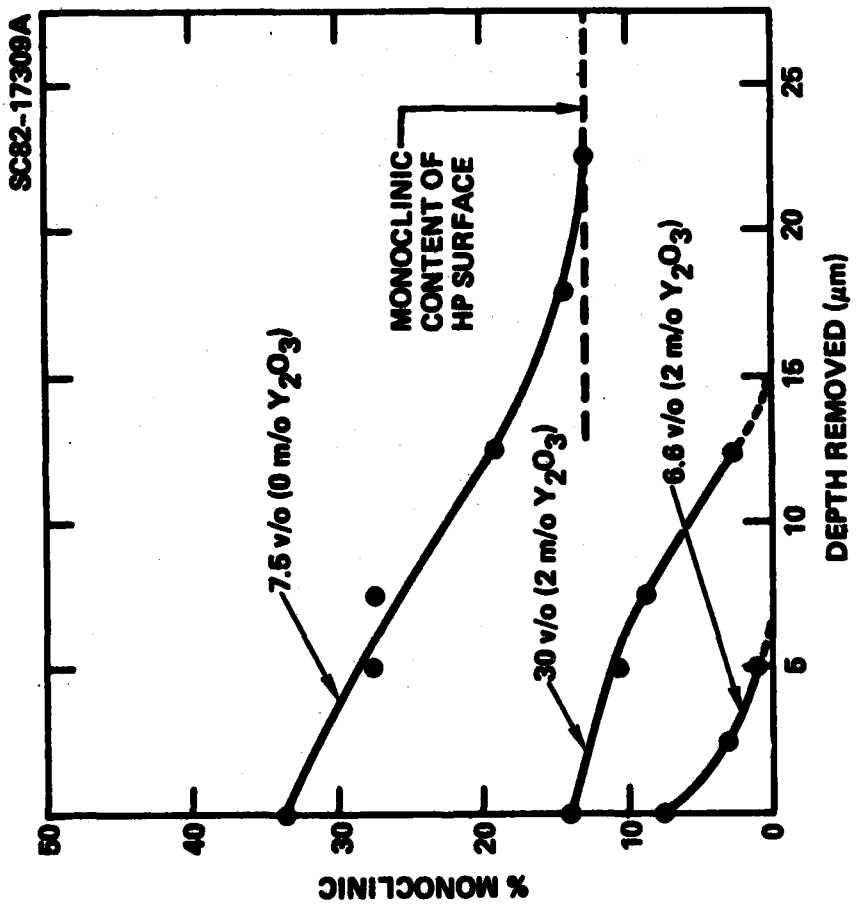


Fig. 1 Monoclinic $ZrO_2$ content as a function of depth removed by polishing, for various $Al_2O_3/ZrO_2$ composites.

## 4.2 Surface Stress of Series Alloyed with $CeO_2$

Figure 2 shows that the average compressive stress, determined with the shallower penetrating CrKα radiation, decreases slightly with increasing $CeO_2$ alloy addition to $ZrO_2$. Ground and annealed surfaces are nearly stress-free. Table 4 reports the surface stress for the same ground materials, as determined with the deeper penetrating CuKα radiation (9 and 10 m/o $CeO_2$ materials were not used). The surface compressive stresses at lower $CeO_2$ are smaller relative to CrKα determinations and appear to reverse to tension at higher $CeO_2$ contents; the single determinations made with CuKα radiation lie within the statistical counting errors (± 23 MPa) and may negate this conclusion.

## 4.3 Effect of $ZrO_2$ Grain Size

The average $ZrO_2$ grain size for the $Al_2O_3$/30 v/o $ZrO_2$ (+2.5 m/o $Y_2O_3$) materials sintered at 1600°C/2 hr and heat-treated at 1650°C for 2, 8, 16 and 24 hrs are 1.3 μm, 1.4 μm, 1.8 μ, 2.2 μm and 3.4 μm, respectively. Figure 3 illustrates typical micrographs of the extreme conditions. Figure 4 illustrates the small increase for the average surface compressive stress (CrKα radiation) with increasing grain size.

Figure 5a and 5b illustrate the results of the stress profile experiments carried out on the $Al_2O_3$/30 v/o $ZrO_2$ (+2.5 m/o $Y_2O_3$) composite (CrKα radiation). A polynominal correction was applied to the raw data to compensate for the stress relaxation that occurs when a portion of the surface is removed.[26] These figures show that the compressive stress decreases with increasing distance from the initial ground surface. A residual compressive stress of ~100 MPa still persisted after a large portion of the initial surface was removed, suggesting that the polishing operation may produce some transformation and/or plastic deformation that results in a surface compressive stress.

A comparison of the two sets of data (Fig. 5a and b) show that the larger grain size material (annealed 1650°C/24 hr, ground) produces a slightly deeper compressive stress layer (~18 μm) relative to smaller-grained material (as-sintered, ground) for which the depth was estimated to be ~13 μm. Also note

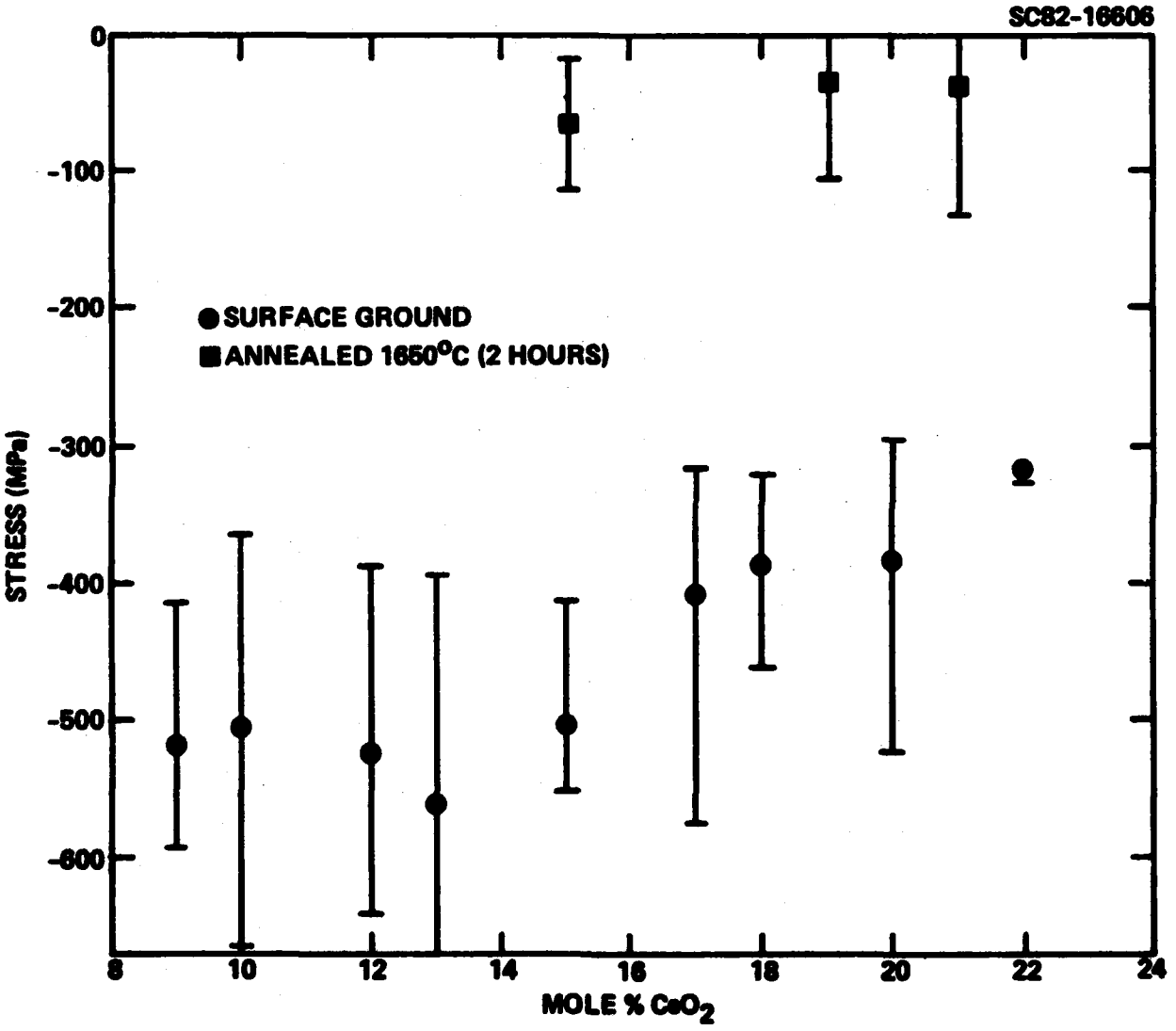


Fig. 2 Surface residual stress measurements for $Al_2O_3$/30 vol% $ZrO_2$ composites, in which $ZrO_2$ is alloyed with various amounts of $CeO_2$. The errors bars represent range of experimental results.

Table 4

Surface Residual Stresses (CuKα Radiation)

| Mole % $CeO_2$ | Surface Stress* (MPa) |
|---|---|
| 12 | -30 |
| 13 | -21 |
| 14 | +17 |
| 15 | + 0 |
| 17 | - 1 |
| 18 | + 2 |
| 19 | +18 |
| 20 | +15 |
| 21 | +21 |
| 22 | +19 |
| Estimated Error ± 23 MPa | |

*Compressive stress is negative.

SC82-19468

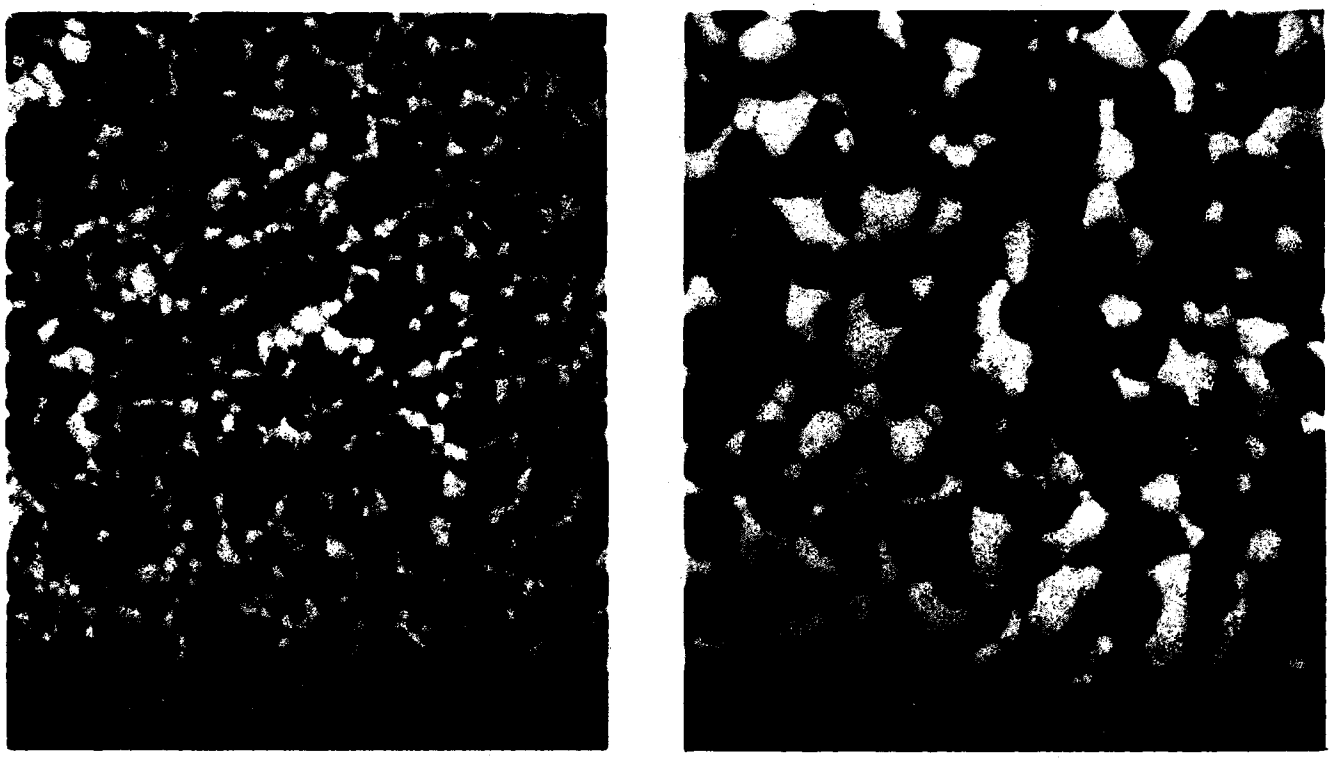

Fig. 3 Comparison of microstructures of $Al_2O_3$/30 vol% $ZrO_2$ composites heat treated; a) 1650°C (2 hours) b) 1650°C (24 hours). Micrograph obtained using backscattered electron mode in SEM.

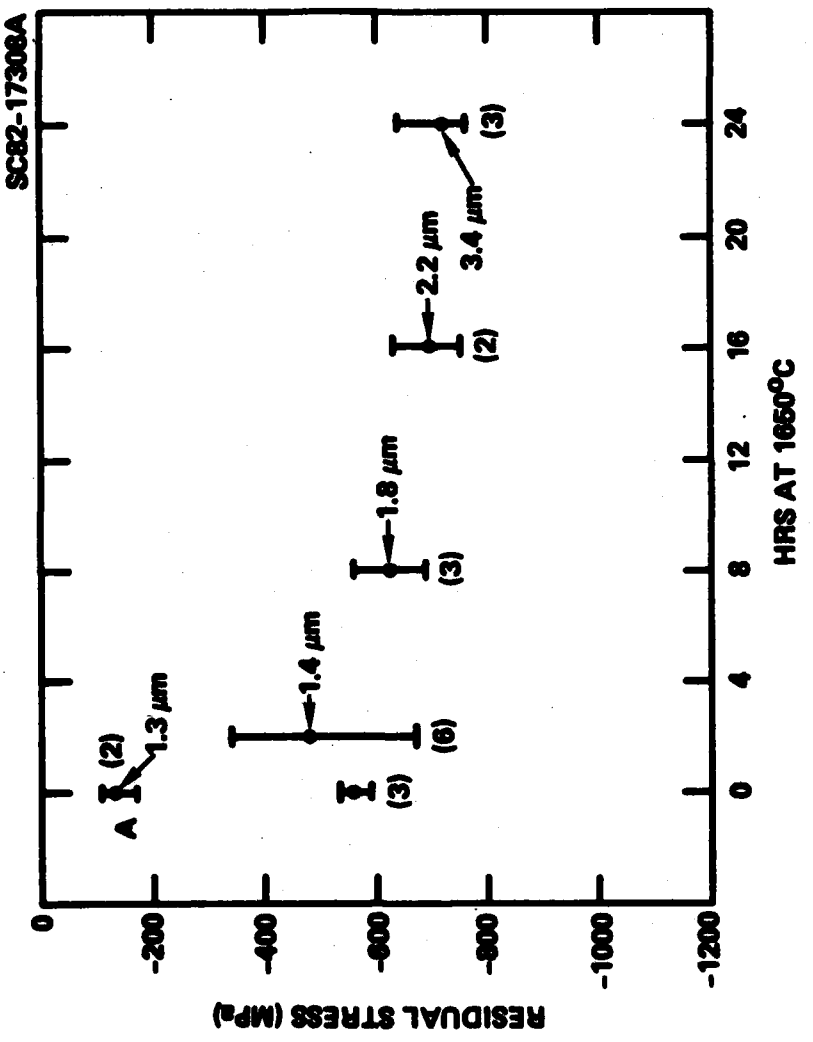


Fig. 4 Surface residual stress measurements for a series of surface-ground $Al_2O_3$/30 vol% $ZrO_2$ specimens heat treated at 1650°C for various times. Included is average $ZrO_2$ grain size and stress determinations on an annealed specimen (A).

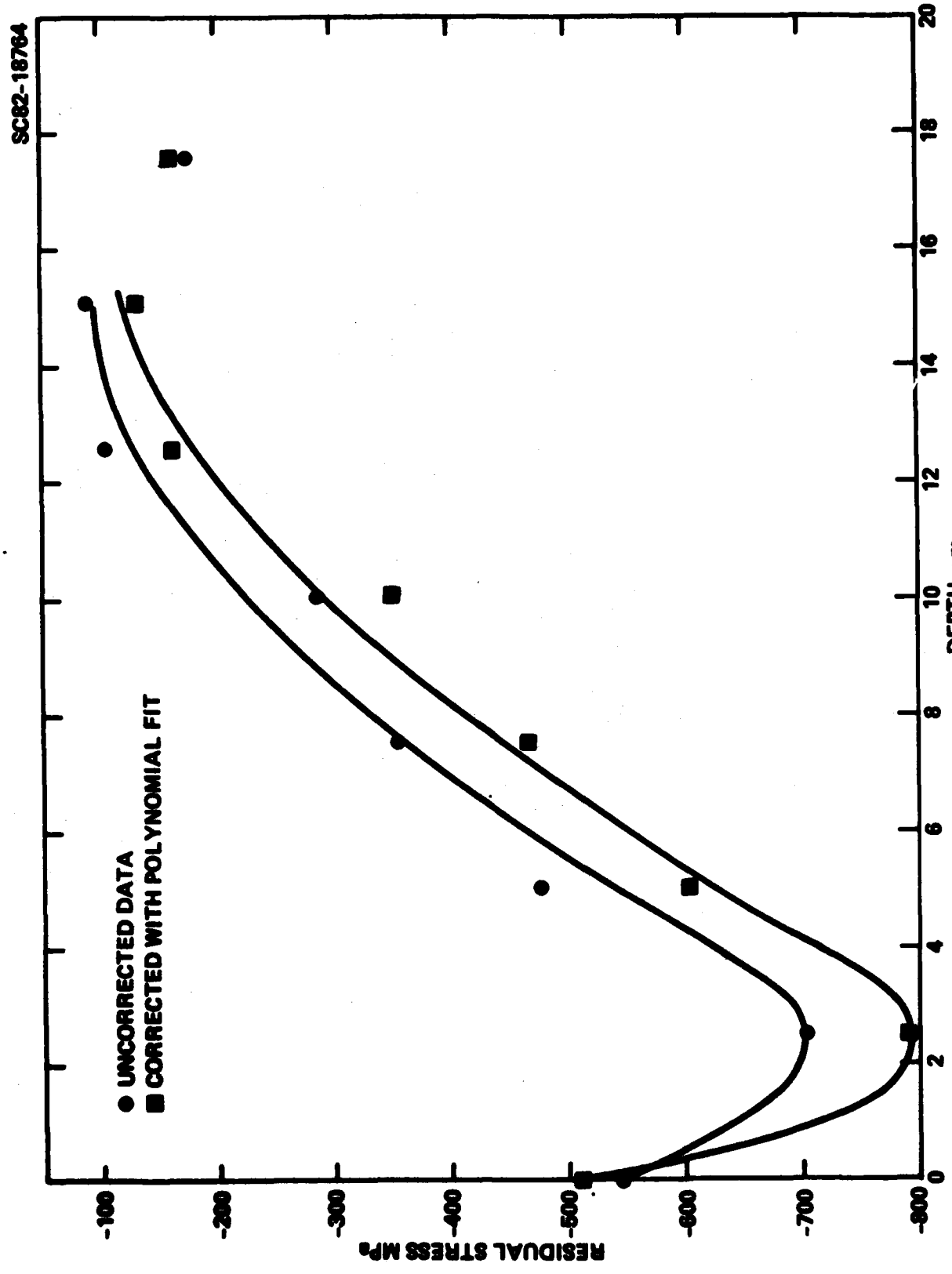


Fig. 5a Experimentally-determined and corrected residual stress profiles for an $Al_2O_3$/30 vol% $ZrO_2$ specimen (Av. $ZrO_2$ grain size, 1.3 μm).

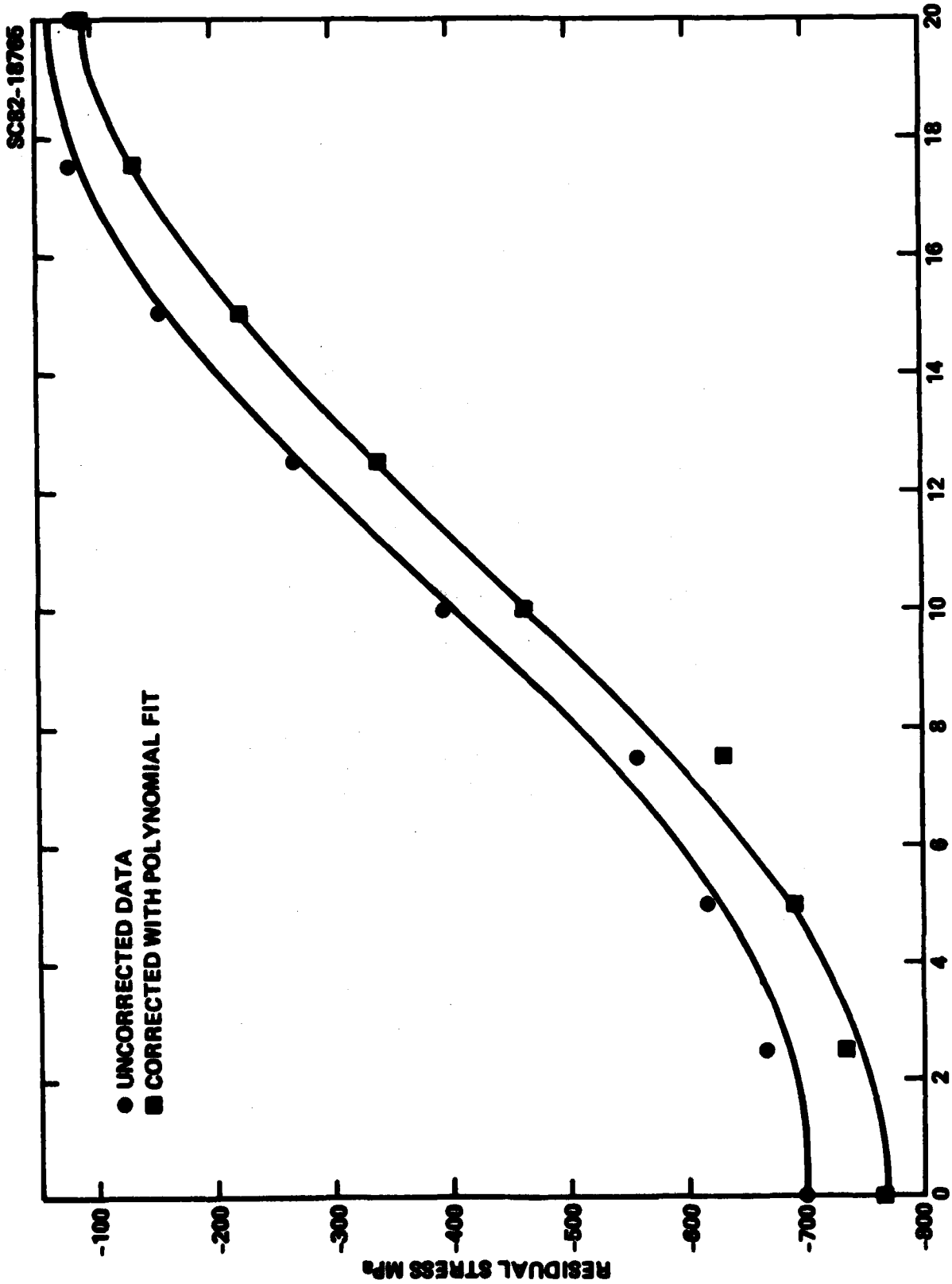


Fig. 5b Experimentally-determined and corrected residual stress profiles for an $Al_2O_3$/30 vol% $ZrO_2$ specimen (Av. $ZrO_2$ grain size, 3.4 μm).

that the depth of the transformed layer for hot-pressed $Al_2O_3$ 30 v/o $ZrO_2$ (+2 m/o $Y_2O_3$) as estimated by successive polishing and XRD measurements (Fig. 1) is nearly identical to compressive larger depths shown in Fig. 5a, which was determined for a nearly identical material (composition and microstructure).

### 4.4 Effect of $ZrO_2$ Volume Fraction

Figure 6 illustrates that the residual compressive stresses (CrKα radiation) increases with increasing v/o $ZrO_2$ retained in the sintered material in its tetragonal structure. Namely, the compressive stress can exceed 1 GPa. It should be noted that these results may be somewhat modified by the fact that $ZrO_2$ is a strong absorber of x-rays (see Table 1). That is, the depth sampled with the CrKα radiation for 7.5 v/o $ZrO_2$ is about three times that for the 60 v/o $ZrO_2$, which may bias the apparent stress magnitude to higher values with increasing $ZrO_2$ content.

## 5. Discussion

All evidence suggests that the residual compressive surface stresses introduced by grinding $Al_2O_3/ZrO_2(t)$ composites are produced by the molar volume change associated with the $ZrO_2(t) \rightarrow ZrO_2(m)$ transformation. In all materials examined, the stresses applied to the surface by the abrasive grinding media were sufficient to induce this transformation as indicative of both XRD phase examination and surface stress determinations. As indicated by comparative results for CuKα and CrKα radiation, the magnitude of the residual surface stress was dependent on the penetration depth of the diffracting x-rays. As suggested by Eq. (1), the magnitude of these residual compressive surface stresses are primarily controlled by the volume fraction of tetragonal $ZrO_2$ (Fig. 6).

Although the magnitude of the residual surface stress is primarily controlled by the $ZrO_2(t)$ volume fraction, data indicates that the depth of the transformed material and the residual stress profile depends on $|\Delta G_c|$ and grain size, D, which determine the critical applied stress required to induce the transformation. As discussed in Section 2, the tranformed depth should increase with increasing $|\Delta G_c|$ and/or $ZrO_2$ grain size (D).

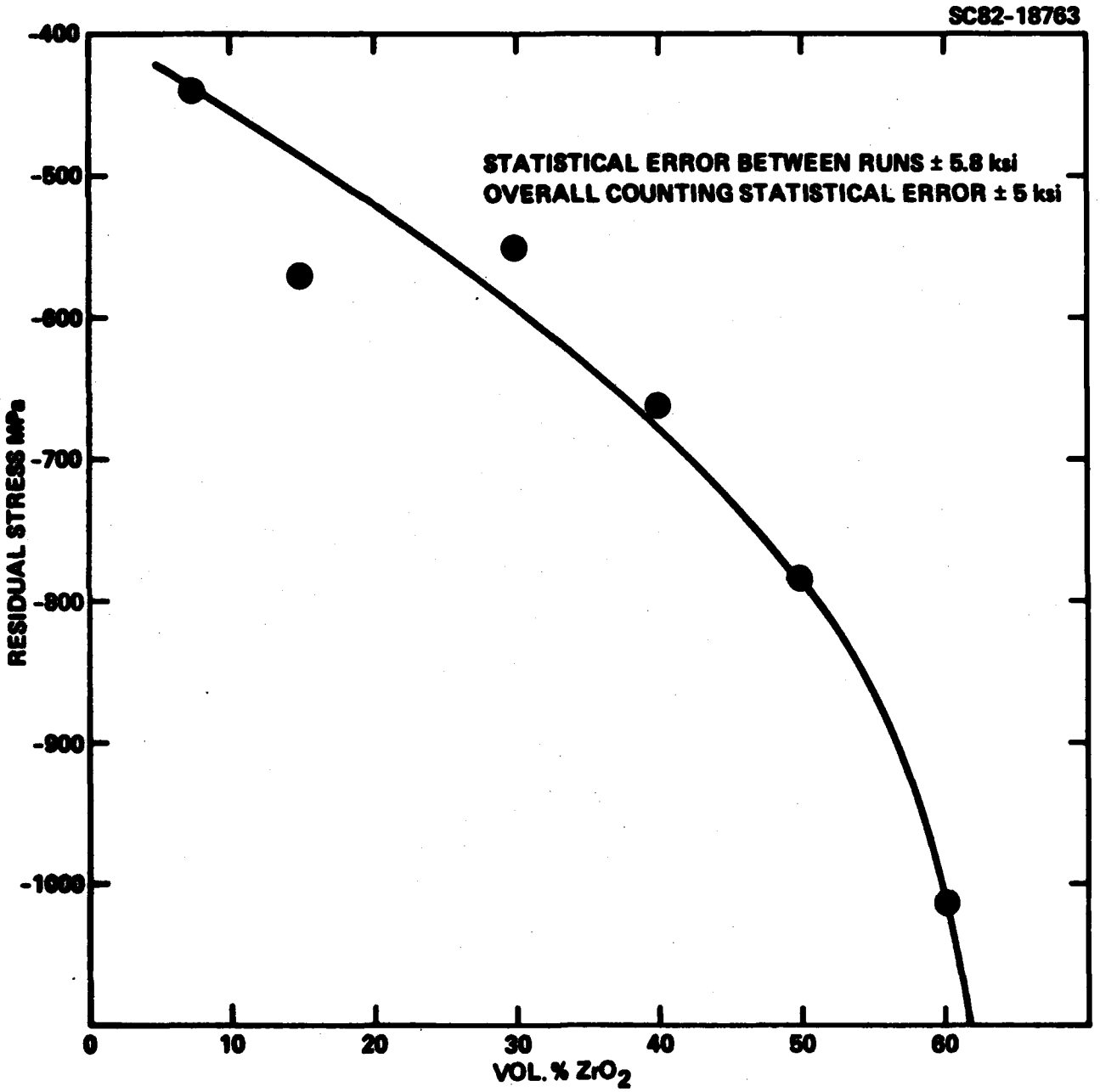


Fig. 6 Average residual surface stress measurements for a series of $Al_2O_3/ZrO_2$ composites.

Both $Y_2O_3$ and $CeO_2$ decrease $|\Delta G_c|$ at room temperature. Figure 1 shows that for nearly equivalent $ZrO_2$ contents (6.6 v/o vs 7.5 v/o), the depth of the transformation layer was much shallower for the case where the $ZrO_2$ was alloyed with the $Y_2O_3$. When $CeO_2$ was alloyed with the $ZrO_2$, residual compressive stresses were only observed with the CuKα radiation for materials with the least $CeO_2$ content, whereas the residual stress exhibited only a slight decrease with increasing $CeO_2$ content when determined with the shallower penetrating CrKα radiation.

Equation (8) also suggests that the depth of the transformed layer should also increase as $D \rightarrow D_c$. Data presented in Fig. 7 is consistent with this hypothesis, i.e., the transformation depth for the material examined increased from ~13 μm to ~18 μm for a grain size increase of 1.3 μm to 3.4 μm.

Further stress profiling experiments are now underway to better substantiate the dependence of the transformation depth on $|\Delta G_c|$ and grain size, D.

## ACKNOWLEDGEMENTS

The authors would like to acknowledge the financial support of the Office of Naval Research, Contract No. N00014-77-C-0441 and the technical assistance of Milan Metcalf.

## REFERENCES

1. H.P. Kirchner, R.M. Gruver and R.E. Walker, "Chemical Strengthening of Polycrystalline Alumina," J. Am. Ceram. Soc., 51 [5] 252-55 (1968).

2. H.P. Kirchner, R.E. Walker and D.R. Platts, "Strengthening Alumina by Quenching in Various Media," J. Appl. Phys., 42 [10] 3685-9 (1971).

3. H.P. Kirchner, R.M. Gruver and R.E. Walker, "Strengthening Alumina by Glazing and Quenching," Am. Ceram. Soc. Bull., 47 [9] 798-802 (1968).

4. F.F. Lange, "Compressive Surface Stresses Developed in Ceramics by an Oxidation-Induced Phase Change," J. Am. Ceram. Soc., 63 [1-2] 38-40 (1980).

5. R.C. Garvie, R.H. Hannink and R.T. Pascoe, "Ceramic Steel?" Nature (London), 258 [12] 703-4 (1975).

6. R.T. Pascoe and R.C. Garvie, "Surface Strengthening of Transformation-Toughened Zirconia," pp. 774-84 in Ceramic Microstructures '76, edited by R.M. Fulrath and J.A. Pask, Westview Press, Boulder, Colorado, 1977.

7. J.S. Reed and A. Lejus, "Effect of Grinding and Polishing on Near-Surface Phase Transformations in Zirconia," Mater. Res. Bull. 12 [10] 949-54 (1977).

8. N. Claussen, "Stress-Induced Transformation of Tetragonal $ZrO_2$ Particles in Ceramic Matrices," J. Am. Ceram. Soc., 61 [1-2] 85-86 (1978).

9. D.J. Green and F.F. Lange, "Influence of Residual Surface Stresses on the Strength of $ZrO_2$ Ceramics," Paper 28-BN-79F, Fall Meeting of Basic Science and Nuclear Divisions of Am. Ceram. Soc., New Orleans, 1979.

10. T.K. Gupta, "Strengthening by Surface Damage in Metastable Tetragonal Zirconia," J. Am. Ceram. Soc., 63 [1-2] 117 (1980).

11. N. Claussen and M. Rühle, "Design of Transformation-Toughened Ceramics," pp. 137-63 in Advances in Ceramics, Vol. 3, edited by A.H. Heuer and L.W. Hobbs, Am. Ceram. Soc., 1981.

12. D.J. Green, Unpublished work.

13. O. Richmond, W.C. Leslie and H.A. Wriedt, "Theory of Residual Stresses Due to Chemical Concentration Gradients," A.S.M. Trans. Q, 57 [1] 294-300 (1964).

14. F.F. Lange, "Transformation Toughening, Part 1," J. Mater. Sci., 17 [1] 225-234 (1982).

15. J.D. Eshelby, "Determination of the Elastic Field of an Ellipsoidal Inclusion and Related Problems," Proc. R. Soc., London, 241A 376-96 (1957).

16. R.W. Davidge and T.J. Green, "The Strength of Two-Phase Ceramic Glass Materials," J. Mater. Sci., 3 [6] 629-34 (1963).

17. M.E. Hilley, J.A. Larson, C.F. Jatczak and R.E. Ricklefs (eds.), Residual Stress Measurements by X-ray Diffraction, SAE Information Report J784a, SAE, Warrendale, Pennsylvania.

18. M.R. James and J.B. Cohen, "The Measurements of Residual Stresses by X-Ray Diffraction Techniques," in Treatise on Materials Science and Technology, 19A ed. H. Hermon, Academic Press, NY, 1-62 (1980).

19. J.F. Nye, Physical Properties of Crystals, pp. 143-5, Oxford at the Clarendon Press, London, 1957.

20. H. Dolle, "The Influence of Multiaxial Stress States, Stress Gradients and Elastic Anisotropy on the Evaluation of Residual Stresses by X-Rays," J. Apply. Cryst., 12, 489-501 (1979).

21. M.R. James and J.B. Cohen, "Study of the Precision of X-ray Stress Analysis," Denver Conference on Advances in X-ray Analysis, 20 (ed. H.F. McMurdie), Kendal/Hunt Publishing Co., Dubuque, Iowa, 291-307 (1977).

22. G. Simmons and H. Wang, Single Crystal Elastic Constants and Calculated Aggregate Properties: A Handbook, p. 146, MIT Press, Cambridge, Mass. (1971).

23. F.F. Lange, "Transformation Toughening: Part 5," J. Mater. Sci., 17 [1] 255-62 (1982).

24. I.A. Aksay, B.I. Davis and F.F. Lange, "Development of Uniformity in $Al_2O_3/ZrO_2$ Compositesd by Colloidal/Filtration Route," (to be published).

25. F.F. Lange, "Transformation Toughening: Part 4," J. Mater. Sci., 17 [1] 247-54 (1982).

26. J.B. Cohen, H. Dolle, and M.R. James, "Stress Analysis from Powder Diffraction Patterns," Proc. Symposium on Accuracy in Powder Diffraction, June 11-15, 1980, National Bureau of Standards, Gaithersburg, Maryland, NBS Spec. Publ. 567, 453-478 (1980).

TECHNICAL REPORT NO. 15

# COMPRESSIVE SURFACE STRENGTHENING OF BRITTLE MATERIALS

D.J. Green

# COMPRESSIVE SURFACE STRENGTHENING OF BRITTLE MATERIALS

D.J. Green
Structural Ceramics Group,
Rockwell International Science Center
Thousand Oaks, CA 91360

## ABSTRACT

A theoretical approach has been put forward for predicting the strengthening of materials by the introduction of surface compressive stresses. An approximate technique was used to determine the closure length of a surface crack which extend through the compressive surface layer. The stress intensity factor of the partially closed crack was then determined for the case of an applied tensile stress with the assumption that the residual surface compressive stress was uniform within the surface layer. The analysis shows that the strengthening depends on the magnitude and depth of the compressive surface stress and the strength of the body in the absence of the residual stress.

# I. INTRODUCTION

The strength of ceramics or glasses can often be increased by placing their surfaces into compression. These techniques include ion exchange, tempering, glazing, surface chemical reactions and stress-induced phase transformations. Although most of these techniques are well-recognized, a theoretical approach to optimization of the strengthening has not been developed. The aim of this paper is to use fracture mechanics to predict the amount of strengthening obtained for a particular residual stress distribution and in particular, to identify the important material and process parameters that need to be controlled. Such an approach would be expected to be relatively straightforward as many crack loading geometries have been solved. The presence of residual stresses does, however, lead to complications in the analysis, when the crack is only partially open at the failure condition and these difficulties have impeded the theoretical developments. Partial crack closure in simple configurations have been analyzed by several authors,[1-5] while for more complex situations numerical approaches have been used.[6-10] In this paper a simplified approach to the crack closure problem for surface cracks is used and the stress intensity factor is then derived in a more rigorous fashion. The amount of strengthening is then determined by inserting the appropriate fracture criterion, thus identifying the important parameters.

## II. THEORETICAL APPROACH

Consider an infinitely-long isotropic plate, width W, which is subjected to the residual stress distribution shown in Fig. 1. This problem is a limiting case of an analysis by Oel and Frechette,[11] and it can be shown that the surface ($\sigma_c$) and interior ($\sigma_t$) stress are given by

$$\sigma_c = \frac{-E\,\varepsilon}{(1-\nu)}\left(\frac{W-2t}{W}\right) \quad \text{for } t > X > (W-t) \tag{1}$$

and

$$\sigma_t = \frac{2E\varepsilon t}{(1-\nu)W} \quad \text{for } t < X < (W-t) \tag{2}$$

where E is the Young's modulus, $\nu$ the Poisson's ratio and $\varepsilon$ is the linear strain associated with the uniform volume change that occurs at the surface. As can be determined from Eqs. (1) and (2), a volume increase at the surface leads to a surface compressive stress and a compensating interior tensile stress. Such a residual stress distribution is expected to be a reasonable approximation for many glazing, enamelling or sealing operations. For the situations where the surface layers are a different material than the inside Eqs. (1) and (2) become slightly more complicated.[11]

The production of ceramic bodies with a compressive surface layer is expected to lead to strengthening, as the compressive stress will oppose applied tensile stresses, particularly when fracture occurs from flaws at or near the surface. When the flaw is completely subjected to the compressive stress the increase in strength of the body ($\Delta\sigma_f$) will be simply given by

$$\Delta\sigma_f = -\sigma_c \quad . \tag{3}$$

In many cases, however, it is expected that the flaw size will be greater than the depth of the compressive zone and it is important to be able to predict the amount of strengthening that will occur. As can be seen from Eq. (1) this will

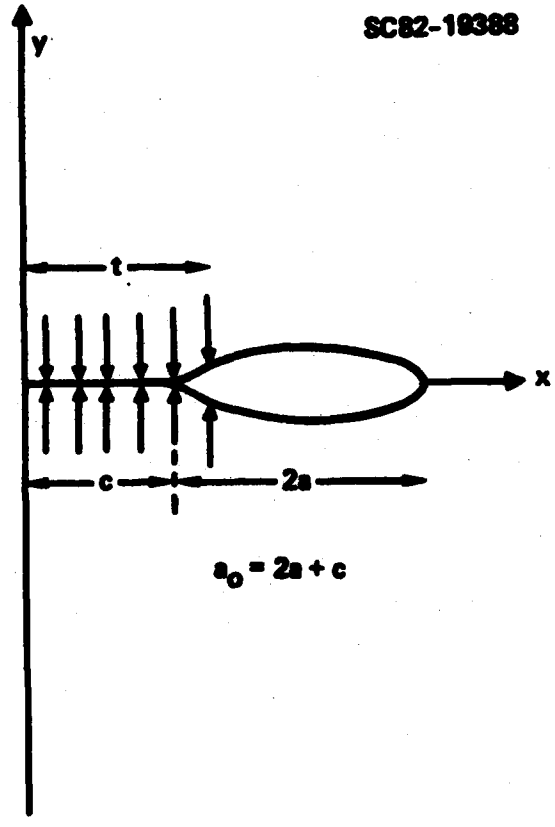


Fig. 1 Residual stress distribution in isotropic flat plate, in which surface has undergone a uniform volume increase.

lead to an optimization process, as the more shallow the depth of the compressive zone, the larger is the surface compressive stress.

Consider now a semi-infinite body containing a surface crack, length $a_0$. For this situation the residual stress distribution will be given by

$$\sigma_c \cong \frac{-E\,\epsilon}{(1-\nu)} \quad \text{for } t > x > (W - t) \tag{4}$$

and

$$\sigma_t \cong 0 \qquad \text{for } t < x < (W - t) \quad . \tag{15}$$

For situations where the surface layers are a different material, the elastic constants in Eq. (4) refer to the surface material. In the absence of an applied stress, the residual stress will act to close the crack so that its surfaces are in contact. For example, it is expected that the crack surfaces will be in contact to a depth t, or for $t/a_0 > 1$, the crack will be completely closed. When a tensile stress is applied to the body the crack will begin to open until at a critical applied stress the crack surfaces will no longer be in contact. The primary intent in this paper is to consider situations when $t/a_0 < 1$ and in particular to derive the stress intensity factor ($K_I$) for this configuration. In this way, it will then be possible to determine the strengthening in terms of $t/a_0$. In order to do this, however, it is necessary to compute the amount of crack closure as a function of the residual and applied stresses.

## A. Crack Closure Analysis

A partially-closed surface crack is illustrated in Fig. 2. For the residual stress distribution being considered, the surface crack is assumed to open from its tip back to the surface under the action of an applied stress. This is reasonable when $t/a_0 < 1$, as considered in this analysis. It should, however, be noted that when $t/a_0 > 1$, the lower constraint at the surface would

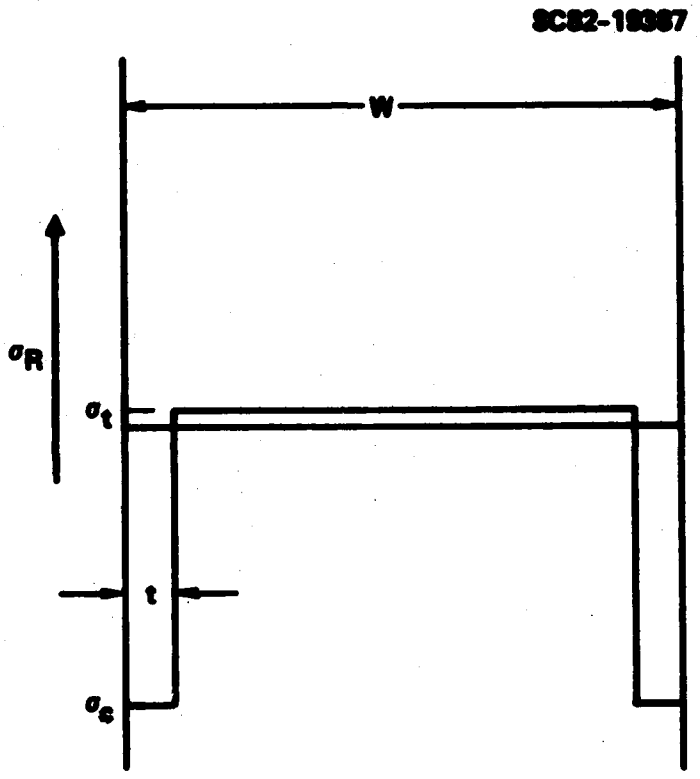


Fig. 2 Surface crack in semi-infinite plate with partial crack closure due to the surface compression.

probably lead to the crack opening in the opposite direction. For these situations, however, the strengthening should be simply given by Eq. (3).

It has been noted by other workers[3,5,8,9] that the stress intensity factor at contact zone (left hand crack tip in Fig. 3) will be zero. It is then possible with this condition to determine the crack closure length (c). This procedure is relatively complex, but for this work a simple solution will be used that was derived by Barenblatt.[12] This solution is strictly only valid for an internal crack in an infinite body but as will be shown later it gives a reasonable description of the closure length. In terms of Fig. 3 the closure distance is givey by[12]

$$\frac{a}{a + (t - c)} = \cos\left[\frac{\pi \sigma_a}{2\sigma_c}\right] \tag{4}$$

where $\sigma_a$ is the applied tensile stress. Using $2a = a_0 - t$, one obtains

$$c_1 = \frac{(1 + t_1)\cos\alpha - (1 - t_1)}{2\cos\alpha} \tag{5}$$

where $c_1 = c/a_0$, $t_1 = t/a_0$ and $\alpha = \pi\sigma_a/2\sigma_c$. Equation (5) is illustrated in Fig. 3. It can be seen that the crack becomes completely open at a critical value of $(\sigma_a/\sigma_c)$ which depends on $(t_1)$. As indicated earlier, the analysis is not expected to be value as $t_1 > 1$. This is reflected in Eq. (5), which becomes independent of the applied stress for $t_1 = 1$. For values of $t_1 > 1$, it is simply assumed that the crack is completely closed until $\sigma_a = -\sigma_c$ and then it becomes completely open. It should also be noted that the use of Eq. (4) ignores the effect of the free surface of the closure length, this is expected to be important as $c_1 \to 0$. For these conditions, however, the crack will be almost completely open and provided the stress intensity factor solution approaches that of an open crack, the approximation should be reasonable.

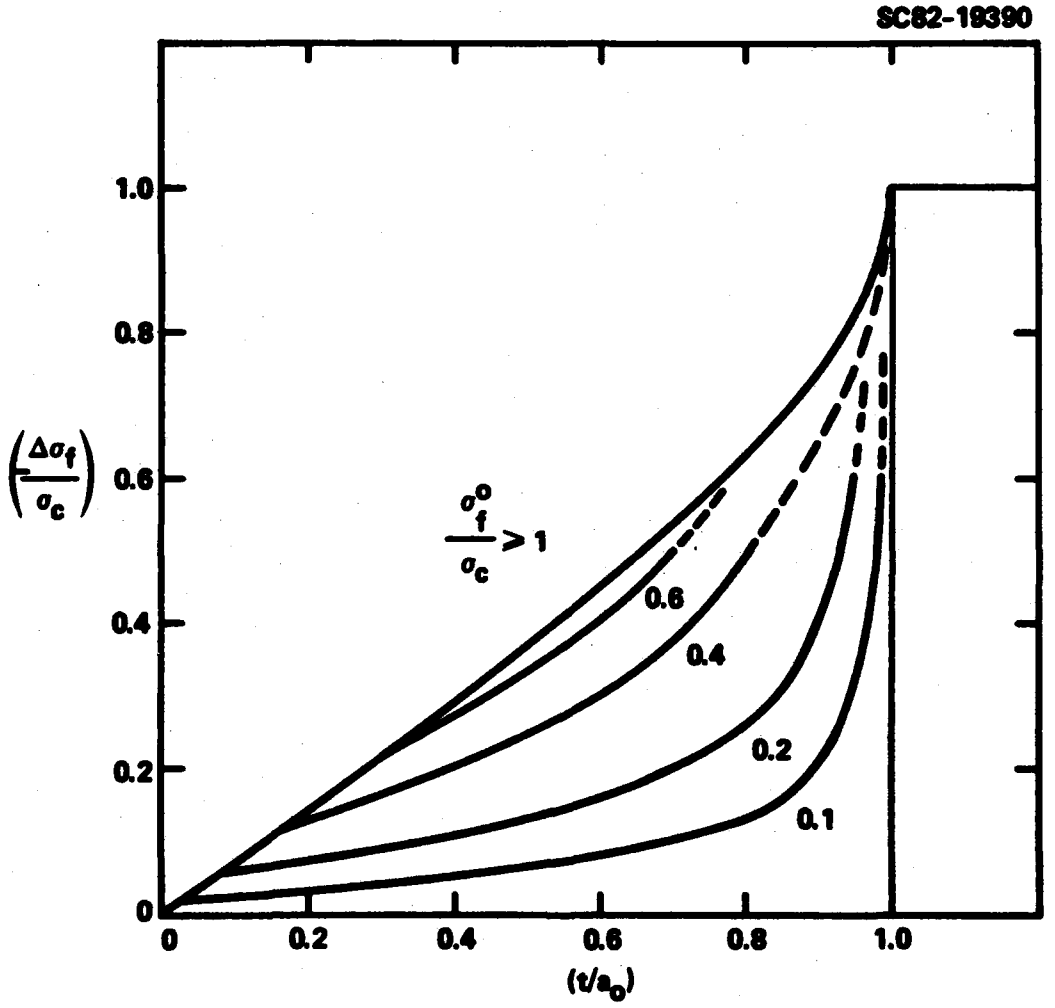


Fig. 3 Crack closure length as a function of the compressive zone depth and applied stress.

B. Calculation of Stress Intensity Factor

For a partially-closed internal crack, length $2a_o$, it has been shown that[2]

$$K_I = 2\left(\frac{a_o}{\pi}\right)^{1/2}(1 - c_1^2)^{1/2} \int_{c_1}^{1} \frac{\sigma(x_1)\, x_1\, dx_1}{\sqrt{[(1 - x_1^2)(x_1^2 - c_1^2)]}} \tag{6}$$

where $x_1 = x/a_o$ and $\sigma(x_1)$ is the prior stress acting along the plane of the crack. The coordinate axes are located so the plane of the crack lies along $y = 0$ and the center of the crack is at $x = 0$. In order to apply this solution to that of a surface crack, the effect of the free surface should be included. This is ususally accomplished by modifying the stress distribution, i.e.,[13]

$$K_I = 2\left(\frac{a_o}{\pi}\right)^{1/2}(1 - c_1)^{1/2} \int_{c_1}^{1} \frac{\sigma(x_1)\, f(x_1)\, x_1\, dx_1}{\sqrt{[(1 - x_1^2)(x_1^2 - c_1^2)]}} \tag{7}$$

where

$$f(x_1) = 1.2945 - 0.6857\, x_1^2 + 1.1597\, x_1^4 - 1.7627\, x_z^6 + 1.5036\, x_1^8 - 0.5094\, x_1^{10} \tag{8}$$

For the residual stress distribution given by Eqs. (4) and (5) and an applied tensile stress, Eq. (7) can be re-written as

$$K_I = 2\left(\frac{a}{\pi}\right)^{1/2}(1 - c_1^2)^{1/2} \int_{c_1}^{t_1} \frac{(\sigma_a + \sigma_c)\, f(x_1)\, x\, dx_1}{\sqrt{[(1 - x_1^2)(x_1^2 - c_1^2)]}} + \int_{t_1}^{1} \frac{\sigma_a f(x_1) x_1\, dx_1}{\sqrt{[(1 - x_1^2)(x_1^2 - c_1^2)]}} \tag{9}$$

Now if we substitute

$$x_1^2 = c_1^2 - (1 - c_1^2)\, u^2 \tag{10}$$

and expand $f(x_1)$ in terms of $u^2$, i.e.,

$$f(x_1) = \sum_{k=0}^{5} \alpha_{2k} u^{2k} \tag{11}$$

one obtains

$$K_I = 2 \left(\frac{a_o}{\pi}\right)^{1/2} (1 - c_1^2) \sum_{k=0}^{5} \alpha_{2k} \int_0^{t_2} \frac{u^{2k}(\sigma_a + \sigma_c)du}{\sqrt{(1 - u^2)}} + \int_{t_2}^{1} \frac{u^{2k}(\sigma_a)\, du}{\sqrt{(1 - u^2)}} \tag{12}$$

where

$$t_2 = \left(\frac{t_1^2 - c_1^2}{1 - c_1^2}\right)^{1/2} \tag{13}$$

From standard integral tables

$$\int \frac{u^{2k}\, du}{(1 - u^2)^{1/2}} = \frac{(2k)!}{(k!)^2} \left[ - (1 - u^2)^{1/2} \sum_{r=1}^{k} \frac{r!\,(r - 1)!\, u^{2r-1}}{2^{2k-2r+1}\,(2r)!} + \frac{1}{2^{2k}} \sin^{-1} u \right] \tag{14}$$

The final solution for the stress intensity factor is given by

$$K_I = \sigma_c (\pi a_o)^{1/2} (1 - c_1^2)^{1/2} \left[F_1(t_2) + F_2(c_1) \left(\frac{\sigma_a}{\sigma_c} + \frac{2}{\pi} \sin^{-1} t_2\right)\right] \tag{15}$$

where

$$F_1(t_2) = \sum_{k=1}^{5} - \frac{\alpha_{2k}(2k)!(1 - t_2^2)^{1/2}\, \pi}{2(k!)^2} \sum_{r=1}^{5} \frac{r!(r - 1)!\, t_2^{2r-1}}{2^{2k-2r+1}\,(2r)!} \tag{16}$$

and

$$F_2(c_1) = \sum_{k=0}^{5} \frac{\alpha_{2k}\,(2k)!}{(k!)^2\,2^{2k}} \quad . \tag{17}$$

It can be shown that Eq. (15) agrees with several limiting cases. For example, in the absence of a residual stress

$$K_I = 1.1215\ \sigma_a\ (\pi a_o)^{1/2} \tag{18}$$

in agreement for the solutions for a surface crack in an applied tensile stress field.[13] For the condition when $-\sigma_a = \sigma_c$, $(c_1 = 0)$

$$K_I = \sigma_a(\pi a_o)^{1/2}\ [\tfrac{2}{\pi} \cos^{-1} t_1]\ G(t_1) \quad . \tag{19}$$

The solution agrees with that derived for a uniform stress near a crack tip,[13] where

$$G(t_1) = \frac{\pi F_1(t_2)}{2\ \cos^{-1}(t_1)} \tag{20}$$

Finally for $\sigma_a = 0$ and $\sigma_c$ is a tensile stress

$$K_I = \sigma_c(\pi a_o)^{1/2}\ (\tfrac{2}{\pi} \sin^{-1} t_1)\ H(t_1) \tag{21}$$

where

$$H(t_1) = \frac{\pi\ F_1(t_2)}{2\ \sin^{-1}(t_1)} \quad . \tag{22}$$

This solution agrees with previous solutions[14,15] for $0 < t_1 < 1$, in which a surface crack has a uniform stress near the free surface.

In order to determine the condition for strengthening the fracture condition the fracture condition must be used, i.e., $K_I = K_c$. Using this condition and $K_c = 1.1215\ \sigma_f^0\ (\pi a_0)^{1/2}$ where $\sigma_f^0$ is the strength ofthe body in the absence of residual stress, Eq. (15) can be rewritten as

$$-\frac{\Delta\sigma_f}{\sigma_c}(1 - c_1)^{1/2} = \frac{F_1(t_2)}{F_2(c_1)} + \frac{2}{\pi}\sin^{-1} t_2 + \frac{\sigma_f^0}{\sigma_c}\ (1 - c_1^2)^{1/2}$$

$$-\frac{1.1215\ \sigma_f^0}{F_2(c_1)\ \sigma_c} \qquad (23)$$

This equation is presented as Fig. 4 and will be discussed in the following section. In the analysis it was found that for $\sigma_f^0/\sigma_c > 1$, the crack will be completely open at failure and the value of $\Delta\sigma_f/\sigma_c$ depends only on $t/a_0$. It was found, however, that as $c/a_0 \to 0$ in situations where $\sigma_f^0/\sigma_c < 1$, the analysis was in error and did not agree with the limiting cases. These problems are presumably a result of the approximate method for determining the closure distance. For values of $t/a_0 > 1$, it was simply assumed that $\Delta\sigma_f/\sigma_c = -1$.

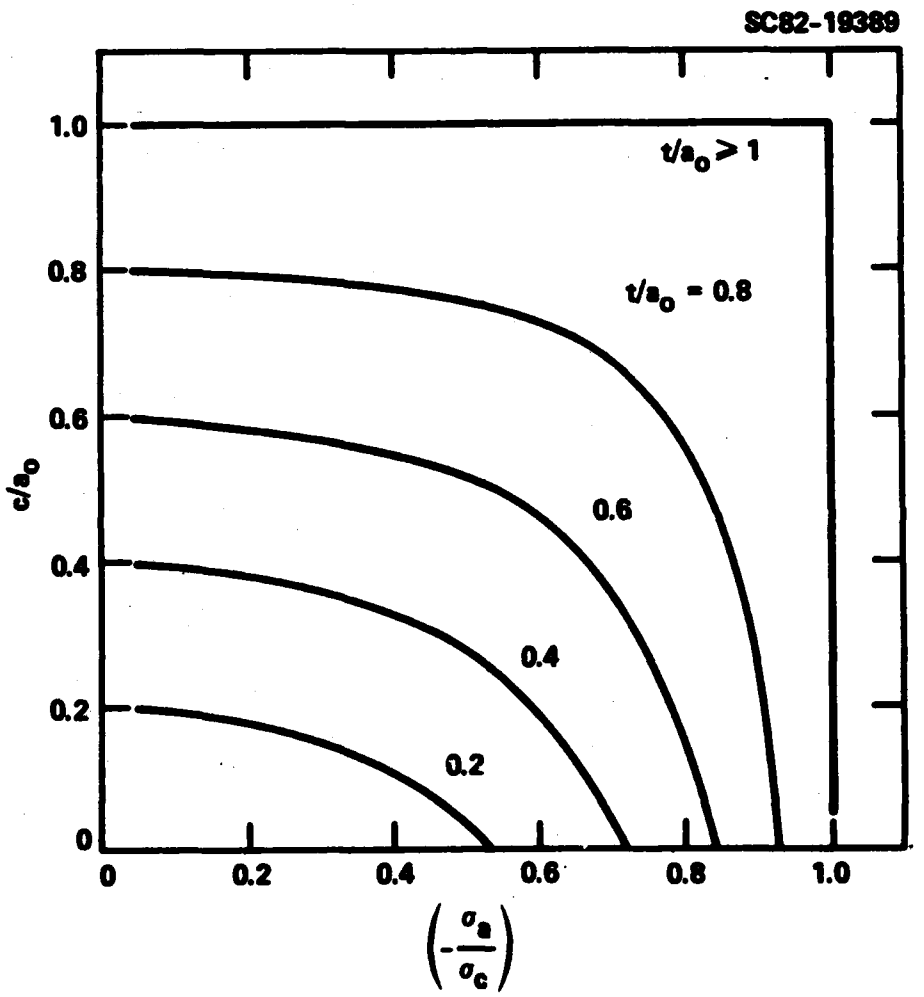


Fig. 4 Strengthening due to surface compression in a semi-infinite plate in terms of compressive stress.

## III. DISCUSSION

The data presented as Fig. 4, have important consequences for optimization of compressive strengthening. For example, for a given value of $\sigma_c$, it is best to have a compressive surface layer that is at least as deep as the surface flaws. In many situations, however, this may not be possible, so for example, at a fixed value of $t/a_o$, the basic strength of the body ($\sigma_f^o$) should be as high as possible. This could be accomplished by increasing the basic fracture toughness of the material. Alternatively decreasing the size of the surface flaws would increase $\sigma_f^o$ as well as increasing $t/a_o$. The strength increase in terms of $\sigma_f^o$ is shown in Fig. 5, which allows us to consider the effect of varying $\sigma_c$ for constant $\sigma_f^o$. It is interesting to note here that increasing $\sigma_c$ for situations where $t/a_o < 1$ does lead to strengthening but the effect saturates as $\sigma_f^o/\sigma_c \to 0$. It should also be remembered that $\sigma_c$ is not necessarily independent of $t/a_o$. For example, increasing the compressive layer depth usually decreases $\sigma_c$. This effect can be seen for example, in Eq. (1). Therefore, in order to use Figs. 4 or 5 for a particular system the variation of $\sigma_c$ with $t/a_o$ must be known and incorporated into the analysis.

Finally, although the production of surface compressive layers is expected to lead to strengthening for materials that fail from surface defects, it must be remembered that if internal flaws act as alternate failure origins, the potential strengthening discussed in this paper, would not be accomplished.

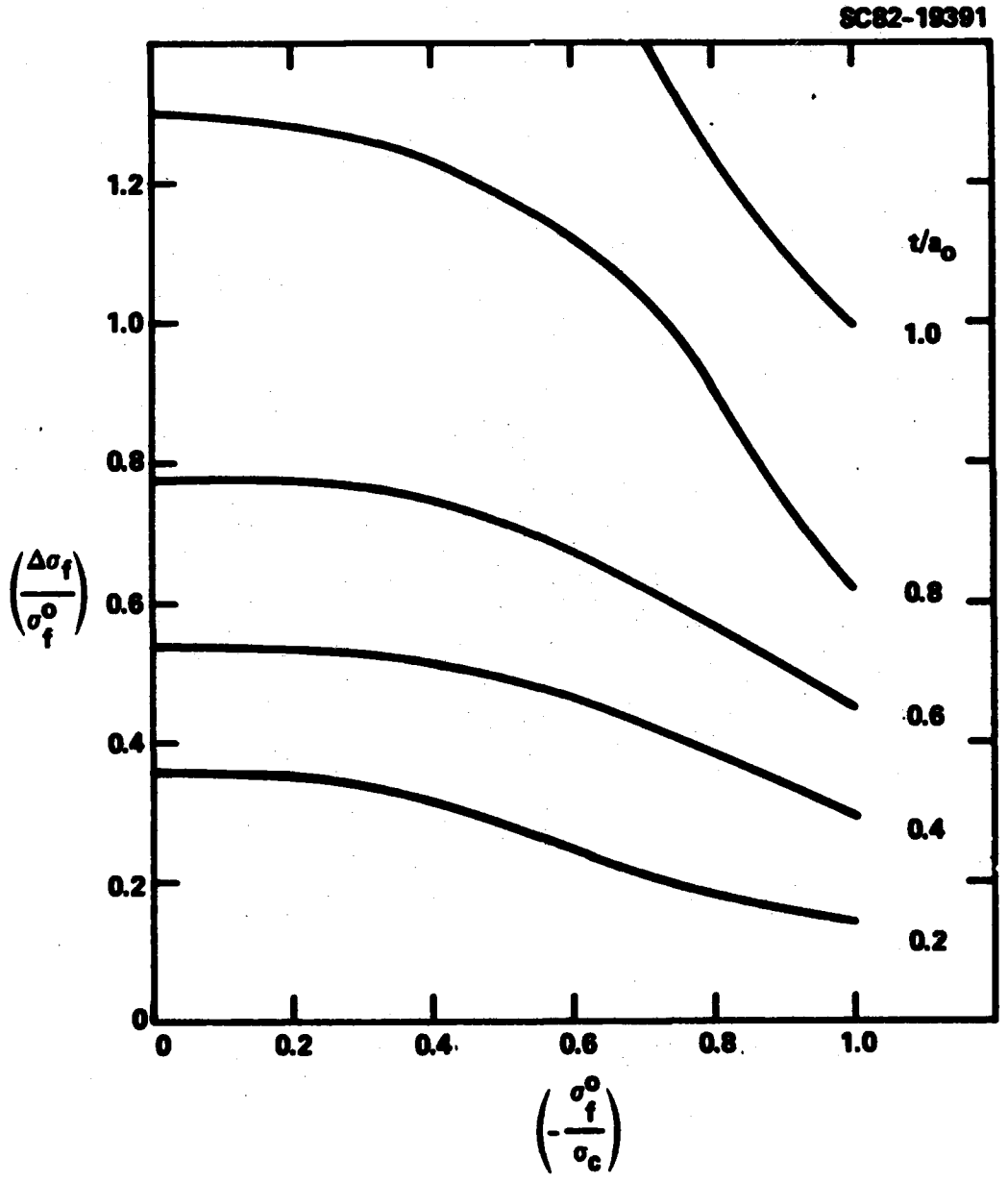


Fig. 5 Strengthening due to surface compression in a semi-infinite plate in terms of base strength of material.

## IV. CONCLUSIONS

An approach has been put forward for predicting the strengthening of a brittle material, when it is subjected to a particular residual stress distribution. The approach involved the calculation of the amount of crack closure and the subsequent determination of the stress intensity factor for the particular configuration. For the cases where a critical surface crack is completely open at the failure condition, the strengthening simply depends on the magnitude of the compressive stress and the ratio of the compressive layer depth to flaw size. In particular, when this ratio > 1, the maximum strengthening is obtained. For situations, however, where the surface crack is only partially open at failure, the amount of strengthening also depends on the basic strength of the material. For example, for a given surface compressive stress, the strengthening can be increased by increasing the base strength of the material. Alternatively, in situations where the base strength cannot be increased, the strengthening can be increased by increasing the magnitude of the compressive stress. This effect, however, saturates at high values of compressive stress. Finally, it was noted that the magnitude of the surface compressive stress depends on the process being used to induce the residual stresses and that failure from an alternate flaw population could reduce the optimum strengthening predicted in this work.

## ACKNOWLEDGEMENTS

The author would like to acknowledge the financial support of the Office of Naval Research, the discussions with Dr. F.F. Lange and Dr. W.F. Hall.

## REFERENCES

1. E.E. Burniston, "An Example of a Partially Closed Griffin Crack," Int. J. Fracture, 5 [1] 17-24 (1969).

2. J. Tweed, "The Determination of the Stress Intensity Factor of a Partially Closed Griffith Crack," Int. J. Engng. Sci., 8 [9] 793-803 (1970).

3. E.E. Burniston and W.Q. Gurley, "The Effect of Partial Closure on the Stress Intensity Factor of a Griffith Crack Opened by a Parabolic Pressure Distribution," Int. J. Fracture 9 [1] 9-19 (1973).

4. R.W. Thresher and F.W. Smith, "The Partially Closed Griffith Crack," Int. J. Fracture 9 [1] 33-41 (1973).

5. O.L. Bowie and C.E. Freese, "On the Overlapping Problem in Crack Analysis" Engng. Fract. Mech., 8 [2] 373-79 (1976).

6. O. Aksogan, "Partial Closure of a Griffith Crack under a General Loading," Int. J. Fracture, 11 [4] 659-70 (1975).

7. O. Aksogan, "Nonhomogeneous Nonsymmetrical Plane Problems with Several Griffith Cracks, One or Two Partially Closed," Int. J. Fracture, 12 [2] 223-30 (1976).

8. M. Bakioglu, F. Erdogan and D.P.H. Hasselman, "Fracture Mechanical Analysis of Self-Fatigue in Surface Compression Strengthened Glass Plates," J. Mater. Sci. 11 [10] 1826-34 (1976).

9. M. Bakioglu and F. Erdogan, "The Crack-Contact and the Free End Problem for a Strip Under Residual Stress," J. Appl. Mech., 44 [1] 41-46 (1977).

10. A.T. Jones and M.L. Callabresi, "Numerical Analysis of the Influence of Residual Stresses on Crack Closure in Rings," Engng. Fracture Mech., 11 [4] 675-88 (1979).

11. H.J. Oel and V.D. Frechette, "Stress Distribution in Multiphase Systems: I Composites with Planar Interfaces," J. Am. Ceram. Soc., 50 [10] 542-49 (1967).

12. G.I. Barenblatt, "The Mathematical Theory of Equilibrium Cracks in Brittle Fracture," pp. 55-126 in Advances in Applied Mechanics, Vol. 7. Edited by H.L. Dryden, Th. Von Karman and G. Kuerti, Academic Press, New York, 1962.

13. R.J. Hartranft and G.C. Sih, pp. 179-238 in Mechanics of Fracture, Vol. 1. Edited by G.C. Sih, Noordhoff Int'l. Publishing, Leyden, The Netherlands, 1973.

14. H. Tada, P.C. Paris and G.R. Irwin, The Stress Analysis of Cracks Handbook, Del Research Corporation, St. Louis, 1973.

15. A.F. Emery, G.E. Walker, Jr., and J.W. Williams, "A Green's Function for the Stress-Intensity Factors of Edge Cracks and Its Application to Thermal Stresses," J. Basic Engng. 91 [4] 618-24 (1969).

TECHNICAL REPORT NO. 16

# TRANSFORMATION TOUGHENING: THERMODYNAMIC APPROACH TO PHASE RETENTION AND TOUGHENING

F.F. Lange

# TRANSFORMATION TOUGHENING: THERMODYNAMIC APPROACH TO PHASE RETENTION AND TOUGHENING

F. F. Lange

Structural Ceramics Group
Rockwell International Science Center
Thousand Oaks, California 91360

## INTRODUCTION

Stress-induced phase transformations can be used to significantly increase the fracture toughness and strength of brittle materials.[1-6] The $ZrO_2$ (tetragonal) → $ZrO_2$ (monoclinic) transformation, which is accompanied by a 3-5% volume increase and a shear strain of ~ 8%,[7,8] has been used to demonstrate this fact. To use the transformation toughening concept, one must first retain the high temperature phase (e.g., $ZrO_2$(t)) by elastic constraint to temperatures below the unconstrained transformation temperature; that is, tetragonal $ZrO_2$ is the toughening agent. Experimental observations have shown that the retention of $ZrO_2$(t) depends on the size of the transforming volume element, viz. a critical grain size or inclusion size must not be exceeded during fabrication. The work done by the loading system to stress-induce the t → m transformation in the vicinity of the crack front is responsible for increasing fracture toughness.

The object here is to review the thermodynamic approach[6] to the conditions required to retain the toughening agent and its contribution to toughening. Although this approach is general for any fast transformation, the t → m transformation will be emphasized. Experimental observations will then be reviewed to compare with theory. Before this is started, four basic microstructures that can be fabricated will be reviewed to set the stage in our discussion, which ultimately relates thermodynamics, microstructures, and properties.

precipitated microstructures can be obtained in large single crystals by Scull melting, as demonstrated by Rice et al,[12] and by sintering powders. The CSIRO Group (Garvie and co-workers)[1,2] have pioneered this sintered microstructure in the $ZrO_2$-CaO system, and the Case-Western Group (Heuer and students)[3] in the $ZrO_2$-MgO system. The sintered microstructures consist of large cubic grains (a result of high temperatures sintering) which contain the internal and grain boundary tetragonal precipitates. The volume fraction of the precipitates is governed by the alloying agent and the heat treatment schedule in the two-phase field.

A second microstructure, consisting of polycrystalline, single phase tetragonal $ZrO_2$, can be fabricated by sintering composite $ZrO_2$ + $Y_2O_3$ (< 3 m/o) powders in the tetragonal phase field, provided that the resulting grain size is less than the critical value (dependent on the $Y_2O_3$ content). Gupta et al[4,5] pioneered this microstructure. Here, neighboring grains constrain one another from the anisotropic transformation strains.

The third microstructure, pioneered by the author,[6] is a two-phase, tetragonal/cubic polycrystalline material in which neighboring grains are either tetragonal or cubic. This microstructure is fabricated by sintering $ZrO_2$ + $Y_2O_3$ composite powders in the two-phase, t + c field. Here again, the tetragonal phase is retained only if the fabricated grain size does not exceed a critical value. The volume content of the tetragonal phase can be varied from 100% to 0% by changing the $Y_2O_3$ content from ~ 3 m/o to ~ 7 m/o.

The fourth microstructure is developed by incorporating $ZrO_2$ into a chemically compatible matrix phase to obtain a polycrystalline, two-phase material by sintering. The $Al_2O_3/ZrO_2$ composite system, pioneered by Claussen,[13] is typical of such systems. Except for very dilute composites (< 10 v/o of the minor phase) on either end of the binary, the composite is itself the constraining matrix. Here, as with other two-phase ceramics, the volume fraction at which the minor phase becomes continuous depends on the dihedral angle. Although the minor phase is primarily located at three and four grain junctions, smaller second phase grains can be observed within the major phase grains indicative of entrapment during grain growth.

Combinations of the above 4 microstructrues are possible.

To generalize, the critical inclusion (or grain) size required to retain the $ZrO_2$ in its tetragonal state depends on the amount and type of alloy added (e.g., $Y_2O_3$, $CeO_2$, MgO, CaO, etc.) to $ZrO_2$, the elastic modulus of the constraining matrix, and the temperature in question. The objective of the next section is to examine the end-point thermodynamics of the constrained transformation in order to put these general observations in an ordered perspective.

**CONDITIONS FOR PHASE RETENTION: THERMODYNAMICS OF A CONSTRAINED TRANSFORMATION (Ref. 6 - Part 1)**

The transformation thermodynamics of an isolated, spherical inclusion constrained by an elastic matrix can be viewed, to the first approximation, by examining the change in free energy ($\Delta G_{t\to m}$) between the initial, untransformed (tetragonal) state and its final, transformed (monoclinic) state; the transformation can only proceed if $\Delta G_{t\to m} < 0$. Although the transformation must satisfy this initial to end-point condition, it should be noted that growth of a transforming nucleus which consumes the inclusion must also satisfy the condition $\Delta G_{t\to m} < 0$ during all stages of growth. Thus, it should be recognized that initial to end-point thermodynamics only estimates transformation conditions, since it neglects "energy barriers" encountered by growing nuclei, viz. it neglects the effect of the initial nucleus size. Even without detailed knowledge of the transformation mechanics and the mechanics of surface phenomena accompanying the transformation, end-point thermodynamics can at least point a direction to uncover the transformation conditions.

For the case when no external stress state is applied to the system, the contribution to the end-point free energy change includes 3 terms: the chemical free energy change ($\Delta G_c$), differential strain energy ($\Delta U_{se}$), and energy changes ($\Delta U_s$) associated with interfacial surfaces and surface phenomena accompanying the transformation. The chemical free energy, $\Delta G_c$, is most dependent on temperatures and alloy content. As indicated in Fig. 1, $\Delta G_c$ is negative below ~ 1200°C for the $ZrO_2$(t) → $ZrO_2$ (m) reaction. Below ~ 1200°C, its absolute value, $|\Delta G_c|$, increases with decreasing temperature. Figure 1 also shows that alloying with $Y_2O_3$ (up to ~ 3.5 m/o) decreases $|\Delta G_c|$ at, e.g., room temperature. Thus, $|\Delta G_c|$ is inversely dependent on temperature and alloy content.

Since the transformation involves a volume change and shear strains, which are constrained by the matrix, a state of stress will arise within both the transformed inclusion and the surrounding matrix. A differential strain energy ($\Delta U^0_{se}$) thus arises from the constrained stress state associated with the transformation. It can be shown that for a given transformation, the magnitude of $\Delta U^0_{se}$ is proportional to the stiffness of the matrix,[6] i.e., the greater the elastic modulus of the constraining matrix, the greater $\Delta U^0_{se}$. It should be noted that $\Delta U^0_{se}$ is always positive. Residual stresses associated with the initial, untransformed state must also be included in the differential strain energy. Such residual stresses can arise as a result of differential thermal expansion before the inclusion attempts to transform. When these residual stresses are included, the total differential strain energy per unit volume can be expressed as[6]

$$\Delta U_{se} = \Delta U^{0}_{se} \pm \sigma^{I}_{ij}\varepsilon^{r}_{ij} \pm \sigma^{r}_{ij}\varepsilon^{t}_{ij} \quad , \tag{1}$$

where $\sigma^{r}_{ij}$ and $\varepsilon^{r}_{ij}$ are the residual stress and strain components associated with the untransformed state, $\sigma^{I}_{ij}$ are the stress components associated with the transformation, and $\varepsilon^{t}_{ij}$ are the unconstrained transformation strains. $\Delta U^{0}_{se}$ is the strain energy only associated with the transformation, i.e.,

$$\Delta U^{0}_{se} = \frac{1}{2}\sigma^{I}_{ij}\varepsilon^{t}_{ij} \quad .$$

Equation (1) illustrates that the residual strains either increase or decrease the strain energy, depending on their sense. For example, if the transformation strains are tensile and the initial residual strains are tensile, the strain energy is diminished. If, on the other hand, the residual strains have a different sense than those associated with the transformation, then the total strain energy differential is increased. As will be shown next, the magnitude of $\Delta U_{se}$ is one factor that controls the constrained transformation temperature.

Before discussing the details and effects of the surface phenomena term, $\Delta U_{s}$, we can sum the three terms to show that the constrained transformation temperature is lower than the unconstrained transformation temperature:

$$\underset{t\to m}{\Delta G} = -|\Delta G_{c}| + \Delta U_{se} + \Delta U_{s} \quad . \tag{2}$$

Since the transformation will not proceed unless $\underset{t\to m}{\Delta G} < 0$, the condition for transformation is

$$|\Delta G_{c}| > \Delta U_{se} + \Delta U_{s} \quad . \tag{3}$$

That is, the contribution of the differential strain energy is to change the transformation temperature. Thus, retention of tetragonal $ZrO_2$ to, e.g., room temperature is possible in a constrained state, provided that the differential strain energy is sufficiently large.

Although $\Delta U_{se}$ is an important term in changing the transformation temperature, the summation of $\Delta G^{c}$ and $\Delta U_{se}$ cannot result in a size effect, i.e., both terms have the same dependence on the volume (or size) of the transforming inclusion. As will be shown, the size effect resides in the surface term, $\Delta U_{s}$.

Three surface phenomena are known to accompany the $ZrO_2(t) \rightarrow ZrO_2(m)$ transformation: interfacial surface change,

twinning, and microcracking. Each will contribute to the differential surface energy and, as will be shown, twinning and microcracking will both alter the differential strain energy.

As Garvie[14] has pointed out, both the surface area and the interfacial surface energy per unit area will change during transformation. Thus, the differential interfacial surface energy per unit volume will have the form

$$\Delta U_{IF} = \frac{A_m\gamma_m - A_t\gamma_t}{V} = \frac{6(\gamma_m - \gamma_t g_s)}{D} \quad . \tag{3}$$

$A_t$ and $A_m$ are the interfacial surface areas of the tetragonal and monoclinic inclusion, $\gamma_t$ and $\gamma_m$ are their respective interfacial surface energies per unit area, and $g_s = A_t/A_m$. For simplicity, the transformed particle is assumed to be a sphere with a volume = $(\pi/6)D^3$ and a diameter D. Thus, when Eqs. (3) and (2) are combined, the interfacial surface term introduces a size effect such that when $\Delta G_{t\to m} < 0$, only those size inclusions with

$$D > D_c^{IF} = \frac{6(\gamma_m - \gamma_t g_s)}{|\Delta G_c| - \Delta U_{se}} \tag{4}$$

can undergo transformation and lower the system's free energy. As shown by Eq. (4), this size effect only occurs at temperatures where $|\Delta G_c| > \Delta U_{se}$.

It will now be shown that the size effects due to twinning and/or microcracking will occur at temperatures where $|\Delta G_c| < \Delta U_{se}$, i.e., these size effects are first encountered upon cooling from the fabrication temperature.

Both twinning (or the formation of invarient planes by the moving transformation front) and microcracking not only introduce new surface energy, but they also relieve a portion of the constraint and thus decrease the differential strain energy. Twinning helps relieve constraint caused by the shape (shear) change associated with the transformation and thus reduces the shear portion of the strain energy by a factor $(1 - f_T)$. Microcracking relieves some constraint due to the volume change and thus reduces the strain energy by a factor $(1 - f_c)$. It can be shown that the summation of the reduced differential strain energy and the differential surface energy as expressed in energy per unit volume for these two surface phenomena are

$$\Delta U_{se} f_T + \frac{6\gamma_T g_T}{D} \qquad \text{for twinning} \tag{5}$$

and

$$\Delta U_{se} f_c + \frac{6\gamma_c g_c}{D} \qquad \text{for microcracking} \tag{6}$$

where $0 < f \leq 1$, $g_T = A_T/A_m$, $g_c = A_c/A_m$, $A_T$ = total area of twins, $A_c$ = total area of crack(s), and $\gamma_T$ and $\gamma_c$ are the respective surface energies per unit area for twin boundaries and microcrack surfaces.

Combining Eqs. (5) and (6) with the chemical free energy change and setting $\Delta_{t\to m} G = 0$, one obtains the critical inclusion size for transformation and twinning:

$$D_c^T = \frac{6(\gamma_T g_T + \gamma_m - \gamma_t g_s)}{|\Delta G_c| - \Delta U_{se} f_T} , \tag{7}$$

which only occurs at temperatures where $|\Delta G_c| > \Delta U_{se} f_T$, and for transformation and microcracking:

$$D_c^c = \frac{6(\gamma_c g_c + \gamma_m - \gamma_t g_s)}{|\Delta G_c| - \Delta U_{se} f_c} , \tag{8}$$

which only occurs at temperatures where $|\Delta G_c| > \Delta U_{se} f_c$.

If the transformation were accompanied by all three surface phenomena, then the critical size becomes

$$D_c^{T,c} = \frac{6(\gamma_T g_T + \gamma_c g_c + \gamma_m - \gamma_t g_s)}{|\Delta G_c| - \Delta U_{se} f_c f_T} . \tag{9}$$

Since Eqs. (4), (7), (8), and (9) are defined for the condition $\Delta_{t\to m} G = 0$, they therefore define a phase boundary in size/temperature space which not only summarize the constrained transformation temperature, but also indicate the accompanying surface phenomena. Thus, when these critical size relations are normalized by the critical size relation for the constrained transformation ($\Delta U_{se} = 0$), viz.

$$D_{uc} = \frac{6(\gamma_m - \gamma_t g_s)}{|\Delta G_c|} , \tag{10}$$

then $D_c/D_{uc}$ can be plotted against $\Delta U_{se}/|\Delta G_c|$ as shown in Fig. 2. Without knowing the values of $f_T$, $f_c$, $g_T$, $g_c$, etc. but knowing their relative magnitudes e.g., $f_c > f_T$, $g_T > g_c$, and $\gamma_c > \gamma_T > \gamma_m - \gamma_t g_s$, one can obtain the phase fields shown in Fig. 2.

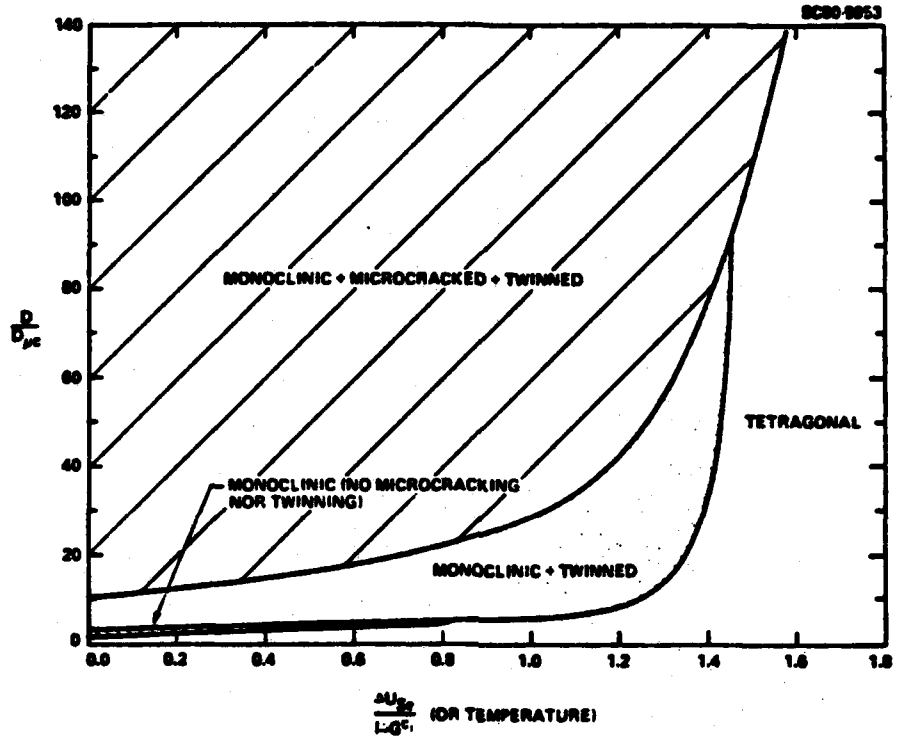


Fig. 2. Phase diagram resulting from surface phenomena accompany transformation.[6]

As detailed elsewhere,[6] the phase diagram shown in Fig. 2 is important to the fabricator who needs to retain the tetragonal phase upon cooling to room temperature. First, it illustrates how surface phenomena that accompany the transformation result in a size effect. Second, it illustrates how the critical size depends on temperature, differential strain energy, and differential chemical free energy. The latter two can be modified by the fabricator to increase the critical size and thus relax the fabrication constraint of grain growth that accompanies sintering and/or heat treatment.

Three examples can be cited where the critical size has been changed in accordance with the thermodynamics leading to Fig. 2. First,[6] alloying $ZrO_2$ with $Y_2O_3$ lowers $|\Delta G_c|$ at room temperature, up to additions of ~ 3.5 m/o, and $Y_2O_3$ thus should increase the critical grain size. Figure 3 shows this effect. Second, increasing the elastic modulus of the constraining matrix, e.g., by incorporating $ZrO_2$ into $Al_2O_3$ ($E_{Al_2O_3}$ = 400 GPa, $E_{ZrO_2}$ = 200 GPa), should increase the critical size. As shown in Table 1,[15] the critical grain size with $Al_2O_3/ZrO_2$ constraining matrix is much larger than for pure $ZrO_2$ and depends on the composite's modulus. Third, one can use both alloying and increased elastic modulus to

increase the critical size. This is demonstrated by adding 2 to 3 m/o $Y_2O_3$ to the $ZrO_2$ and using $Al_2O_3$ as the constraining matrix. Here the critical size is raised above 1 μm for all composite compositions in the $Al_2O_3$-$ZrO_2$ binary.[6] That is, the use of $Y_2O_3$ permits one to fabricate $Al_2O_3/ZrO_2(t)$ composites with much larger volume fractions of $ZrO_2(t)$ without attempting to maintain $ZrO_2(t)$, grain sizes ≤ 0.5 μm.

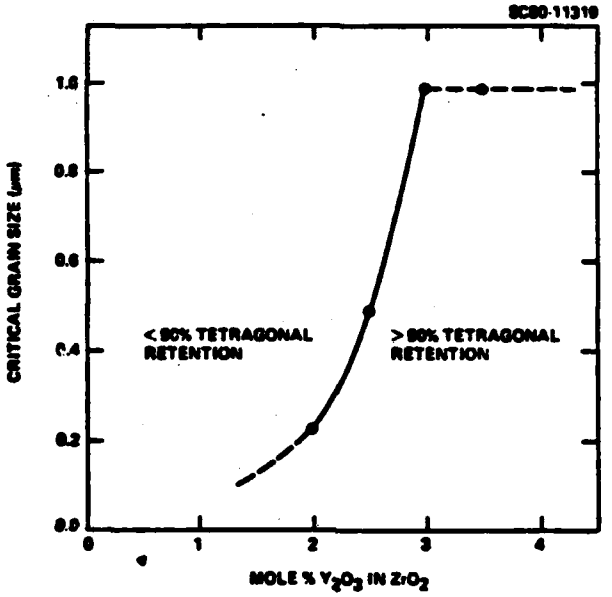


Fig. 3. Critical grain size vs $Y_2O_3$ content.[6]

Table 1. Critical Grain Size for $Al_2O_3/ZrO_2$ Composites[15]

| Vol Fraction $ZrO_2$ | Heat Treatment Temp (°C) | Heat Treatment Time (h) | Critical Grain Size (μm) |
|---|---|---|---|
| 0.05* | 1650 | 12 | >2.3 |
| 0.10 | 1650 | 4 | 1.35 |
| | 1650 | 8 | 1.35 |
| | 1650 | 12 | 1.41 |
| 0.15 | 1650 | 4 | 0.85 |
| | 1650 | 8 | 0.84 |
| | 1650 | 12 | 0.85 |
| 0.20** | 1650 | 4 | 0.74 |

*Monoclinic $ZrO_2$ not detectable by x-ray diffraction.
**Longer heat treatment produced too much monoclinic $ZrO_2$ for reliable results.

## WORK TO STRESS-INDUCE THE TRANSFORMATION

Before examining the fracture toughness contribution, let us first examine the work required to induce a constrained transformation. Again we will consider a spherical inclusion within an elastic matrix. If the stress state ($\sigma_a$) applied by external loads is of the same sense to the transformation strains, a sufficient stress can induce the transformation. Taking the $ZrO_2(t) \rightarrow ZrO_2(m)$ transformation as an example, an applied triaxial tensile stress will unconstrain the volume increase associated with the transformation. As shown by Eshelby,[16] the work per unit volume of transforming material done by the loading system is given by

$$W = \sigma^a_{ij} \varepsilon^t_{ij} \quad , \tag{11}$$

where $\varepsilon^t_{ij}$ are the components of the unconstrained trnsformation strain tension. That is, the potential energy of the loading system is lowered by WV, where V is the transformed volume.

The end-point thermodynamics of this situation can be expressed as (below 1200°C for $ZrO_2$)

$$\underset{t \rightarrow m}{\Delta G} = -|\Delta G_c| + \Delta U_{se} f + \frac{6\Sigma\gamma_g}{D} - W \tag{12}$$

where (1 - f) is the strain energy reduction due to the surface phenomena that relieves stress, and $\Sigma\gamma_g$ are the sum of the surface energy terms for the surface phenomena accompanying the transformation. The minimum work required to stress-induce the transformation is determined when $\underset{t \rightarrow m}{\Delta G} = 0$,

$$W = -|\Delta G_c| + \Delta U_{se} f + \frac{6\Sigma\gamma_g}{D} \quad . \tag{13}$$

Eq. (13) shows that the work per unit volume required to induce the transformation is inversely proportioned to the inclusion size. If we multiply Eq. (13) by the volume of the transforming inclusion ($V = \frac{\pi}{6} D^3$), we can express the total work for transformation as

$$WV = -(|\Delta G_c| - \Delta U_{se} f)\frac{\pi}{6} D^3 + \pi \Sigma\gamma_g D^2 \quad . \tag{14}$$

This function is shown in Fig. 4, illustrating that the minimum work required to stress-induce the transformation is maximized when

## BASIC MICROSTRUCTURES

The $ZrO_2$-$Y_2O_3$ binary system[9,10,11] (Fig. 1) will be used to illustrate how 3 of the 4 basic microstructures that include the tetragonal $ZrO_2$ toughening agent are fabricated. As shown, $Y_2O_3$ forms a solid solution with $ZrO_2$ ($Zr_{1-x}Y_xO_{2-x/2}\square_{x/2}$) to reduce the t → m transformation temperature from ~ 1200°C for pure $ZrO_2$ to ~ 600°C for the eutectoid composition containing ~ 3.5 m/o $Y_2O_3$.* Additions of > 7 m/o $Y_2O_3$ stabilize the cubic structure to room temperature.

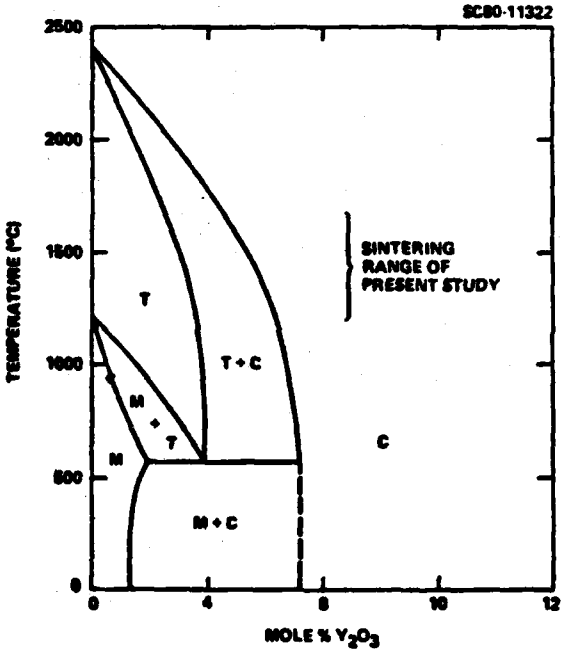


Fig. 1. $ZrO_2$-$Y_2O_3$ system.[9,10,11]

One microstructure that can be produced is obtained by fabricating $ZrO_2$ containing ~ 3 to 7 m/o $Y_2O_3$ in the high temperature cubic phase field, and then quenching into the two-phase (tetragonal + cubic) field to precipitate tetragonal inclusions from the cubic matrix. If the inclusions do not grow to exceed a critical size, the two-phase material can be cooled to room temperature to retain the inclusions in their tetragonal structure. Such

*m/o = mole %; v/o = volume %.

$$D = D_{max} = \frac{4\Sigma\gamma_R}{|\Delta G_c| - \Delta U_{se}^{\ell}} \quad . \tag{15}$$

Figure 4 also illustrates that no work is required to induce the transformation when $D = D_c$, i.e., the constrained transformation is spontaneous without an applied stress when $D > D_c$. Comparing Eq. (15) with those relations derived for the critical inclusion size for spontaneous transformation, one obtains a relation between $D_{max}$ and $D_c$:

$$D_{max} = \frac{2}{3} D_c \quad . \tag{16}$$

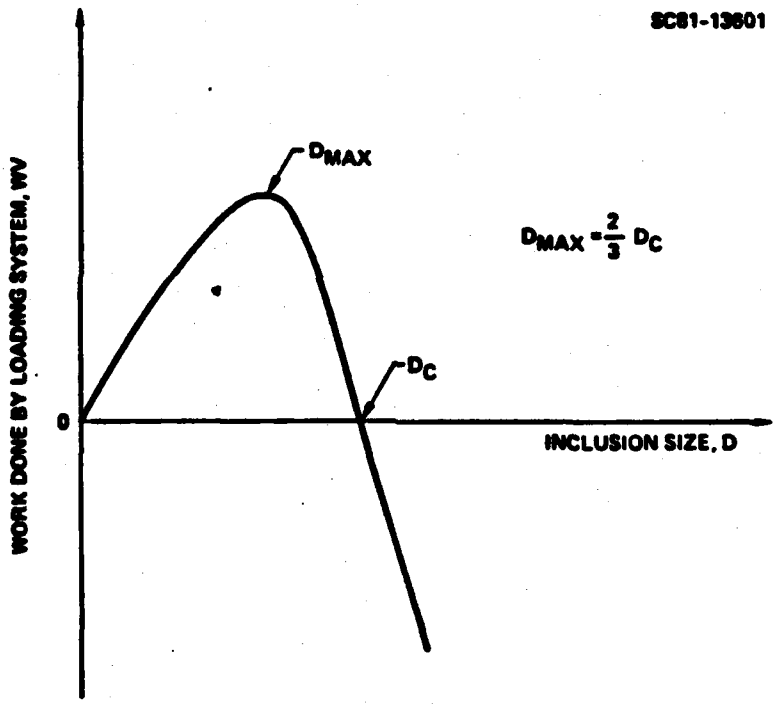


Fig. 4. Work done vs inclusion size.

Thus when the various surface phenomena that accompany the constrained transformation are incorporated into the end-point thermodynamics, one not only obtains a critical size effect for an unstressed, spontaneous transformation as illustrated in the last section, but also an inclusion size which maximizes the work required to stress-induce the transformation.

CONTRIBUTION TO FRACTURE TOUGHNESS[6]

The crack shielding approach to fracture toughness, which is also in a state of theoretical development, will not be reviewed here. This approach attempts to calculate the stress at the crack front to induce the transformation and then the stress-intensity solution of the crack shielded by the compressive stress field arising from the transformed material adjacent to the crack surfaces. Readers are referred to Evans et al.[17] The approach outlined here concerns the thermodynamics of stress-induced transformation and crack extension.

Consider a pre-existing crack loaded in normal tension located in a material containing constrained inclusions of tetragonal $ZrO_2$. Under a sufficient load, the tensile and shear stresses at the crack front unconstrained the inclusions to cause them to transform. The loading system, through the crack's stress field does work during this stress-induced transformation. If crack extension were to occur and material transformed by the stress field were to remain in its transformed state once the stress field of the crack has moved on, then the work required for the transformation would be lost to the fracture process. That is, the stress-induced transformation contributes to increasing fracture toughness. The question is, how large is this contribution and under what conditions can this contribution be optimized.

From a thermodynamic view point, material adjacent to the crack front that stays in its transformed state once the crack's stress field is removed must be in a state of lower free energy relative to its initial constrained tetragonal state. Using the Irwin[18] approach, i.e., where one determines the work to close a crack by a unit length, we can calculate the work required to retransform material adjacent to the crack front back to its tetragonal state and the work to close the crack.

Let us consider a crack under fixed grip conditions which has stress induced and then transversed an inclusion. The residual strain energy associated with the inclusion is $\Delta U_{se} f$, where $\Delta U_{se}$ is the strain energy change associated with transformation, and $(1 - f)$ is that portion of the strain energy relieved by the traversing crack. One might imagine that inclusions closer to the newly formed crack surface contain less strain energy than those far from the free surface. The first force field we apply reverts the fractured inclusion back to its tetragonal state. The work per unit volume performed by this first force field is

$$W = |\Delta G_c| - \Delta U_{se} f \quad ,$$

where $|\Delta G_c|$ is the change in chemical free energy for the monoclinic to tetragonal transformation. One can see that the more

the inclusion is unconstrained by the fracture process, the smaller $\Delta U_{se}f$ and the greater the work. The total work done on all inclusion with the crack tip volume ($2R\Delta A$) is

$$\Delta W_t = 2R\Delta A V_i W = 2RV_i(|\Delta G_c| - \Delta U_{se}f)\Delta A \quad . \tag{17}$$

$V_i$ is the volume fraction of inclusion; R is the radius of the transformed zone adjacent to the crack front.

Once the inclusions are reverted to their tetragonal state, the strain energy associated with their transformed state disappears, and the crack now looks like an ordinary crack in a two-phase material. At this point, the second force field is applied to close the crack. As defined by Irwin,[18] the critical work performed in this operation is

$$\Delta W_c = G_o \Delta A \quad , \tag{18}$$

where $G_o$ is the critical strain energy release rate for the composite material without the transformation phenomenon.

The total work for crack closure per unit crack length which also reverts the inclusions to their initial tetragonal state is thus

$$\frac{\Delta W}{\Delta A} = G_c = G_o + 2RV_i(|\Delta G_c| - \Delta U_{se}f), \tag{19}$$

or, expressed as the critical stress intensity factor for the transforming composite,

$$K_c = \left(\frac{E_c G_c}{(1-\nu_c^2)}\right)^{1/2} = \left(K_o^2 + \frac{2RV_i E_c(|\Delta G_c| - \Delta U_{se}f)}{(1-\nu_c^2)}\right)^{1/2} \quad . \tag{20}$$

This result shows that the contribution of the stress-induced transformation is proportional to the volume fraction of the tetragonal phase ($V_i$), the elastic modulus of the composite ($E_c$), the difference between the chemical free energy change and the resudual strain energy ($|\Delta G_c| - \Delta U_{se}f$), and the size of the transformation zone (R).

Experimental results for each of these factors will be reviewed in the next section.

## FRACTURE TOUGHNESS: EXPERIMENTAL

### Volume Fraction of Retained Tetragonal $ZrO_2$

Two different series of materials have been fabricated to investigate the effect of volume fraction of the retained tetragonal phase on fracture toughness. The first series was fabricated in the $ZrO_2$-$Y_2O_3$ system in which the $Y_2O_3$ content was increased from 2.5 m/o to 7.5 m/o in order to traverse the tetragonal/cubic phase field in Fig. 1. Figure 5 illustrates $K_c$ vs $Y_2O_3$ content which can be transformed directly to $K_c$ vs $V_f$ ($ZrO_2(t)$) from XRD analysis of these two-phase materials.[6] As illustrated, $K_c$ increases with increasing volume content of $ZrO_2(t)$.

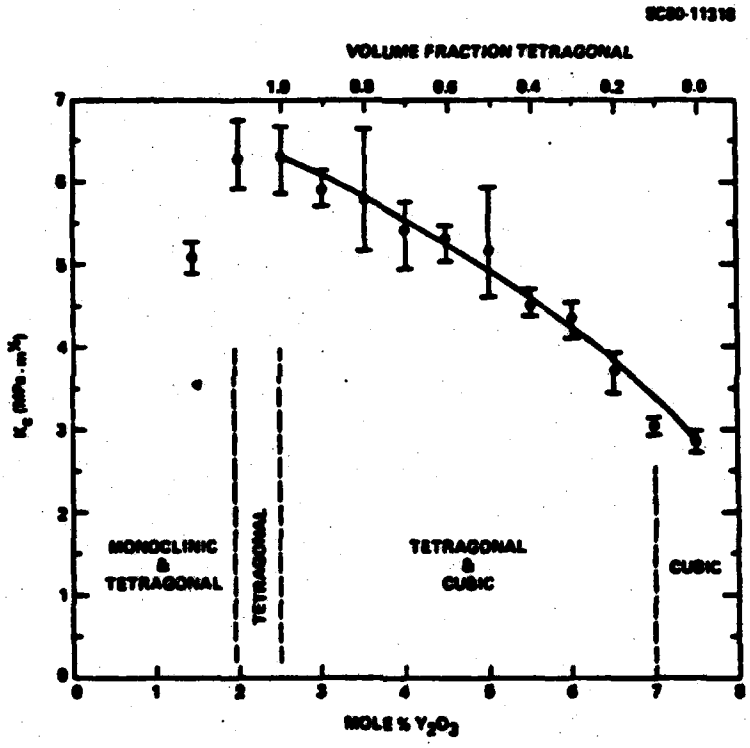


Fig. 5. $K_c$ for $ZrO_2(t)/ZrO_2(c)$ composites.[6]

The second series was fabricated in the $ZrO_2$-$Al_2O_3$ system from one end member to the other. $Y_2O_3$ (2 m/o) was incorporated into the $ZrO_2$ in order to increase the critical grain size and allow complete retention of $ZrO_2(t)$ to volume fraction up to ~ 60 v/o $ZrO_2$. Again, up to ~ 60 v/o $ZrO_2$, toughness increases with increasing v/o of $ZrO_2(t)$, as shown in Fig. 6. Figure 6 also illustrates the toughness of the $Al_2O_3/ZrO_2$ (cubic) composite series in which 7.5 m/o $Y_2O_3$ was incorporated with the $ZrO_2$. For this series, toughness decreases from one end-member to the other.

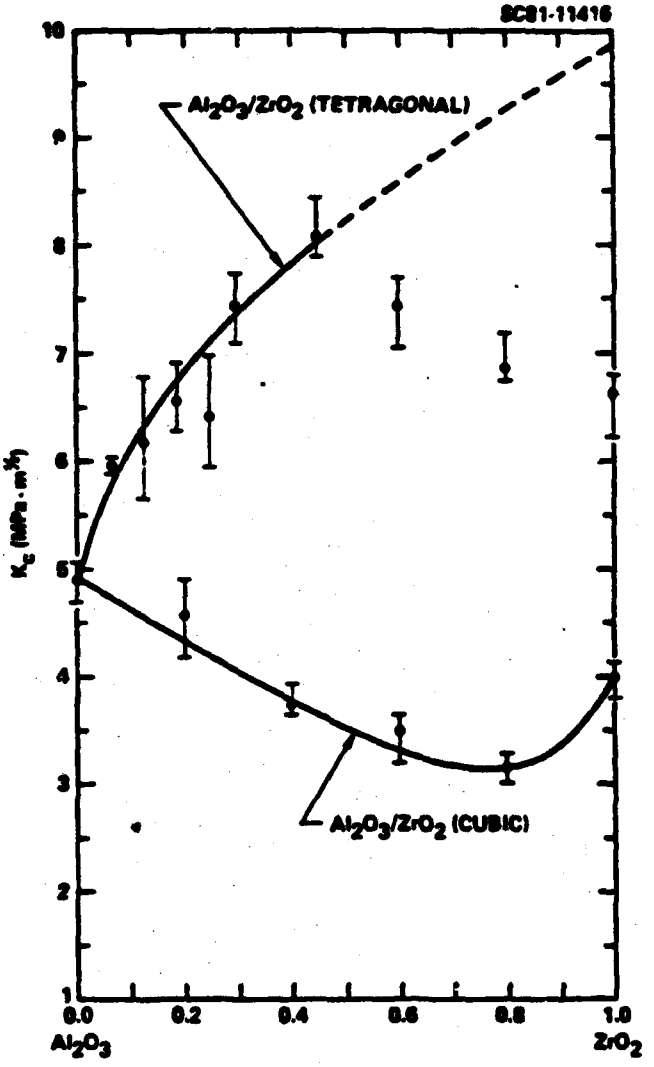


Fig. 6. $K_c$ for $Al_2O_3/ZrO_2$ composites.[6]

Without the $Y_2O_3$ addition to $ZrO_2$, tegragonal $ZrO_2$ can only be completely retained in the $Al_2O_3$ matrix to volume fractions ranging between 10 to 15 v/o $ZrO_2$. For such a series, the $K_c$ vs volume fraction data show a maximum at approximately the same volume fraction which maximizes the tetragonal phase.[16]

Elastic Modulus of Composite

Comparing the data shown in Figs. 5 and 6, one can see that at comparable volume fractions (< 50 v/o $ZrO_2$(t)) more is gained with the high modulus $Al_2O_3/ZrO_2$ constraining matrix. For example, at 30 v/o $ZrO_2$(t) the toughness increase for the $ZrO_2$(c)/$ZrO_2$(t)

composite is ~ 1.5 MPa.$m^{1/2}$, whereas in the $Al_2O_3/ZrO_2$(t) composite the gain is ~ 2.5 MPa.$m^{1/2}$. Detailed comparison with theory is difficult, since all other factors have not been held constant. For example, the end-point solid-solution for the $ZrO_2$ in the $ZrO_2$(c)/$ZrO_2$(t) composites is ~ 3 m/o $Y_2O_3$, whereas it is 2 m/o $Y_2O_3$ in the $Al_2O_3/ZrO_2$(t) series.

## Chemical Free Energy Change[6]

The magnitude of $|\Delta G_c|$ for the $ZrO_2$(t) → $ZrO_2$ transformation decreases with increasing temperature and increasing alloy content. The effect of temperatures on $K_c$ for a single phase $ZrO_2$(t)(+ 2 m/o $Y_2O_3$) and three $Al_2O_3/ZrO_2$(t) composites is shown in Fig. 7. As predicted by theory (Eq. (20)), $K_c$ decreases with increasing temperature. When these data are combined with the known property data ($E_c$,$K_o$ and $V_i$) and Eq. (20) is used to calculate ($|\Delta G_c| - \Delta U_{se}f$) vs temperature, the slope of the function with respect to temperature is nearly identical to that of pure $ZrO_2$.[19] Also, the temperature where ($|\Delta G_c| - \Delta U_{se}f$) = 0 falls within the range of 680°C to 900°C, which is the expected range for t → m transformation of $ZrO_2$ + 2 m/o $Y_2O_3$ (i.e., the temperature where $|\Delta G_c|$ for this composition is zero). These correlations are shown in Table 2. To obtain this agreement, the value of R used in Eq. (20) was chosen as the size of the $ZrO_2$(t) grains. This reasonable corelation suggests that $\Delta U_{se}f$ = 0 and R = the grain size of $ZrO_2$(t) inclusion. If one believes that these two correlations are not fortuitous, then it suggests that those grains closer to the crack surface contribute the most to the tougnening and that the size of this most important transformation zone is equal to the grain size.

Table 2. Values Used to Analyze $K_c$ vs Temperature Data[6]

| MATERIAL | $K_c$ (MPa · $m^{1/2}$) | $K_o$ (MPa · $m^{1/2}$) | $(\|\Delta G^c\| - \Delta U_{se}f)$ (MJ · $m^{-3}$) | $E_c$ (GPa) | $\nu_c$ | $V_i$ | R (μm) | $\frac{\partial(\|\Delta G^c\| - \Delta U_{se}f)}{\partial T}$ (MJ · $m^{-3}$ · $C^{-1}$) | $T_o$ (°C) |
|---|---|---|---|---|---|---|---|---|---|
| $Al_2O_3$/20.3 v/o $ZrO_2$ (+2 m/o $Y_2O_3$) (Hot Pressed) | 7.46 | 4.10 | 100 | 300 | 0.25 | 0.203 | 0.99 | -0.29 | 680 |
| $Al_2O_3$/20 v/o $ZrO_2$ (+2 m/o $Y_2O_3$) (Sintered) | 8.83 | 4.10 | 100 | 333 | 0.25 | 0.20 | 1.53 | -0.27 | 730 |
| $Al_2O_3$/45 v/o $ZrO_2$ (+2 m/o $Y_2O_3$) (Hot Pressed) | 6.30 | 3.70 | 100 | 285 | 0.25 | 0.45 | 1.10 | -0.21 | 900 |
| $ZrO_2$ (+2 m/o $Y_2O_3$) (Hot Pressed) | 6.71 | 3.80 | 100 | 297 | 0.25 | 1.00 | 0.35 | -0.24 | 830 |
| Average of four materials | | | | | | | | -0.25 | 785 |
| $ZrO_2$ (pure)[19] | | | | | | | | -0.25 | 1200 |
| $Zr_{0.98}Y_{0.02}O_{1.99}$ ($ZrO_2$ + 2 m/o $Y_2O_3$)[6,19] | | | | | | | | | 680 - 830 C |

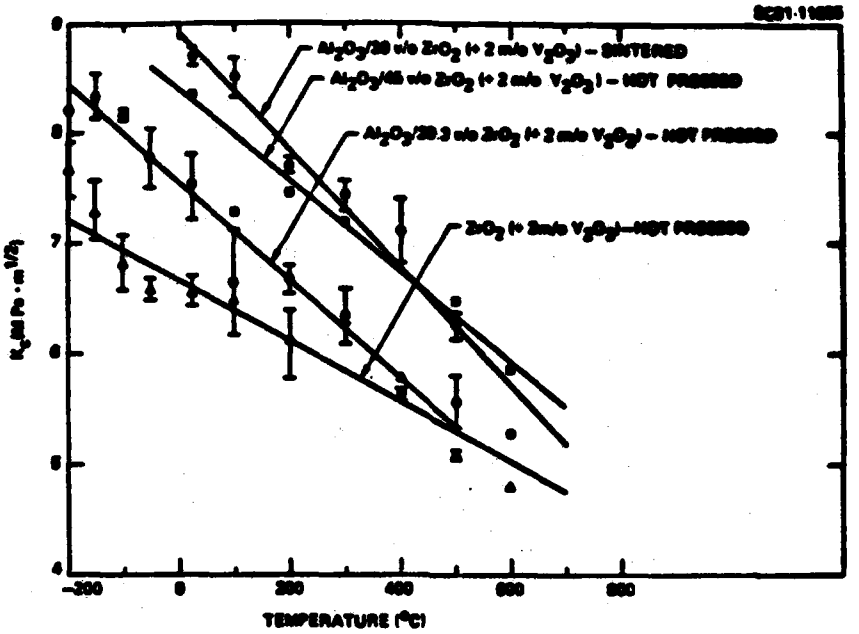


Fig. 7. $K_c$ vs temperature.[6]

The second way to change the magnitude of $\Delta G_c$ is to change the alloy content. Additions of $CeO_2$ were chosen, since the tetragonal phase field extends to ~ 20 m/o $CeO_2$ relative to the smaller phase field in the $ZrO_2$-$Y_2O_3$ binary. Composites containing $Al_2O_3$/30 v/o $ZrO_2$ (+ $CeO_2$) were fabricated by sintering in air. The mole % of $CeO_2$ was varied in 1 m/o increments between 6 m/o and 23 m/o $CeO_2$. Tetragonal $ZrO_2$ was the only $ZrO_2$ phase for $CeO_2$ contents > 12 m/o. As shown in Fig. 8, $K_c$ decreases with increasing $CeO_2$ alloying addition as predicted from Eq. (20). If one extrapolates this data to 0 m/o $CeO_2$, it suggests a value $K_c$ = 10.3 MPa·$m^{1/2}$ for these composite ($Al_2O_3$/30 v/o $ZrO_2$(t)) without the alloying addition.

## Size of Transformation Zone

Various indirect and direct (thin foil, EM) observations suggest that the size of the transformation zone is < 5 μm at room temperature. The above theory suggests that those inclusions closer to the fracture surface are less constrained after transformation and crack extension and thus contribute most to work loss during fracture. For this reason, this author has suggested that R = D. In addition, Section 4 strongly suggests that the work done per inclusion can be maximized by fabricating a material in which $D = 2/3\ D_c$. For these reasons, an $Al_2O_3$/25 v/o $ZrO_2$ (+ 2 m/o $Y_2O_3$) was fabricated to full density at temperatures ranging from 1400°C to 1650°C to increase the size of the $ZrO_2$(t) grains. Although SEM

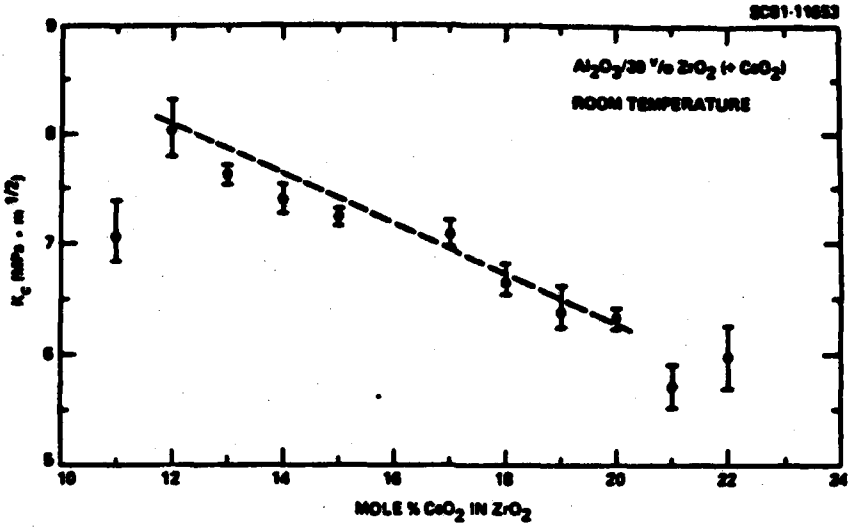


Fig. 8. $K_c$ vs $CeO_2$ content in tetragonal phase field.[6]

micrographs have been taken of etched, polished surfaces to show that the $ZrO_2$ grain size does increase with increasing fabrication temperature, actual grain size determinations have not been made. XRD examinations show that the $ZrO_2$ is all tetragonal regardless of fabrication temperature. Figure 9 illustrates $K_c$ vs fabrication temperature (i.e., $D < D_c$). Although these data are preliminary, they do indicate that $K_c$ increases with increasing grain size (D). They also suggest that a maximum grain size ($D_{max}$) exits for optimum toughness where $D_{max} < D_c$.

## CONCLUDING REMARKS

The end-point thermodynamic approach to retention of tetragonal $ZrO_2$ and its contribution to toughness appears to be useful in explaining observed phenomena. With regard to phase retention, it not only explains why a critical size exists, but also directs the fabricator to possibilities of increasing the critical size to allow phase retention within the constraints (i.e., grain growth) of current fabrication technology. With regard to toughening, it correctly describes the limitation of the transformation toughening concept, i.e., decreasing toughness with decreasing $|\Delta G_c|$ (viz. increased temperature and alloy content). It can thus be seen that there is a competition between phase retention and toughening; conditions for phase retention are relaxed by decreasing $|\Delta G_c|$, but at the same time, decreasing $|\Delta G_c|$ decreases toughness. It has been this author's experience that a resolution of this dilemma is to increase our fabrication skills in limiting grain growth during densification. A solution to this problem would open up the area of using, e.g., the HfO2 transformation, which has a much greater

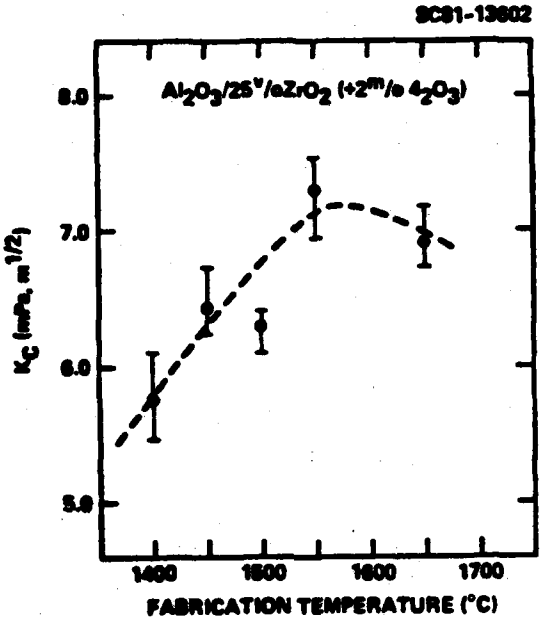


Fig. 9. $K_c$ vs fabrication temperature.

$|\Delta G_c|$ at room temperature than the $ZrO_2$ transformation and would be a much better toughening agent at higher temperatures than tetragonal $ZrO_2$.

It has been amply demonstrated that the transformation toughening concept not only leads to toughening, but also to strengthening, e.g., strengths > 1.2 GPa have been achieved in the $Al_2O_3/ZrO_2$ composite system.[6] At the same time, however, the reader should remember that $K_c$ is only one factor controlling strength, viz. crack size and distribution also controlling strength and strength scatter, but these two factors are mainly controlled by fabrication.

One final remark is in order. The strengthening derived from tetragonal $ZrO_2$ (or some other fast transformation) is due to two phenomena: the toughening due to stress-induced transformation at the crack front and surface compressive stresses induced by the molar volume increase associated with a stress-induced transformation at the surface.[2] Unlike other ceramics, surface machining or particle impact of materials that incorporate tetragonal $ZrO_2$ produces a strengthening effect. The conditions under which this effect can be optimized are certainly worthy of further scientific exploration.

ACKNOWLEDGEMENTS

The work this author has conducted on transformation toughening has been supported by the Office of Naval Research under contract No. N00014-77-C-0441.

REFERENCES

1. R.C. Garvie, R.H. Hannick and R.T. Pascoe, Nature 258, 703 (1975).
2. R.C. Garvie and R.T. Pascoe, Processing of Crystalline Ceramics, ed. by H. Palmour III, R.F. Davis and T.M. Hare, p. 263, Plenum Press (1978).
3. D.L. Porter and A.H. Heuer, J. Am. Ceram. Soc. 60, (1977); ibid. 280 (1977).
4. T.K. Gupta, J.H. Bechtold, R.C. Kuznichi, L.H. Adoff and B.R. Rossing, J. Mat. Sci. 12, 2421 (1977).
5. T.K. Gupta, F.F. Lange and J.H. Bechtold, J. Mat. Sci. 13, 1464 (1978).
6. F.F. Lange, "Transformation Toughening, Parts 1-5," J. Mat. Sci. (in press).
7. E.C. Subbarao, H.S. Maiti and K.K. Srivastava, Phys. Stat. Sol. 21, 9 (1974).
8. A. Heuer and G.L. Nord, Jr., Electron Microscopy in Minerology ed. by H.R. Weuk, p. 274, Springer-Verlag (1976).
9. K.K. Srivastava, R.N. Patil, C.B. Chandary, K.V.G.K. Gokhale and E.C. Subbarao, Trans. Brit. Ceram. Soc. 73, 85 (1974).
10. G.G. Scott, J. Mac. Sci. 10, 1527 (1975).
11. V.S. Stubican, R.C. Hink and S.P. Ray, J. Am. Ceram. Soc. 61, 17 (1978).
12. R. Rice, private communication.
13. N. Claussen, J. Am. Ceram. Soc. 59, 49 (1976).
14. R.C. Garvie, J. Phys. Chem. 69, 1238 (1965); J. Phys. Chem. 82, 218 (1978).
15. F.F. Lange and D.J. Green, Proceeding of Zircona Conf. Case-Western University, Feb. 1981, Am. Ceramics Soc. (in press).
16. J.D. Eshelby, Progress in Solid Mechanics, 2, ed. by I.N. Sneddon and R. Hill, p. 89, North-Holland (1961).
17. A.G. Evans, N. Burlingame, M. Drury and W.M. Kriven, Acta Met. 29, 447 (1981).
18. G.R. Irwin, Hanbuck der Physik, 6, p. 551, Springer, Berlin (1958).
19. E.D. Whitney, J. Am. Ceram. Soc. 45, 612 (1962).